DOI 10.1515/hsz-2013-0244 — Biol. Chem. 2014; 395(3): 253–274

Review

Reinhard Lipowsky*

Remodeling of membrane compartments: some consequences of membrane fluidity

Abstract: Biological membranes consist of fluid bilayers with many lipid and protein components. This fluidity implies a high flexibility that allows the membranes to attain a large variety of different shapes. One important shape parameter is the spontaneous curvature, which describes the asymmetry between the two leaflets of a bilayer and can be changed by adsorption of 'particles' such as ions or proteins from the aqueous phases. Membrane fluidity also implies that the membranes can change their local composition via lateral diffusion and form intramembrane compartments. Two mechanisms for the formation of such compartments can be distinguished: membrane segmentation arising from structured environments and domain formation as a result of phase separation within the membranes. The interplay between these two mechanisms provides a simple and generic explanation for the difficulty to observe phase domains *in vivo*. Intramembrane domains can form new membrane compartments via budding and tubulation processes. Which of these two processes actually occurs depends on the fluid-elastic properties of the domains, on the adsorption kinetics, and on external constraints arising, e.g., from the osmotic conditions. Vesicles are predicted to unbind from adhesive surfaces via tubulation when the spontaneous curvature of their membranes exceeds a certain threshold value.

Keywords: adsorption-induced curvature; domain-induced budding; intramembrane compartments; membrane morphology; spontaneous curvature; spontaneous tubulation.

***Corresponding author: Reinhard Lipowsky,** Theory and Bio-Systems, Max Planck Institute of Colloids and Interfaces, Science Park Golm, 14424 Potsdam, Germany, e-mail: lipowsky@mpikg.mpg.de

Introduction

The primary function of biological membranes is to partition space into different compartments. Thus, all eukaryotic cells contain many membrane-bound organelles and vesicles in addition to their outer cell membranes. The corresponding membrane architecture is dynamic and continuously remodeled by budding and fission processes that create new vesicles from donor membranes and by adhesion and fusion processes that incorporate vesicles into acceptor membranes.

These remodeling processes directly reflect the membranes' molecular design, which is based on *fluid* bilayers that are formed by a complex mixture of lipids and 'decorated' by many proteins. Lipid bilayers are very thin, with a thickness of a few nanometers, but their lateral extension can vary from tens of nanometers to many hundreds of microns or even macroscopic dimensions. If we labeled any two neighboring lipids or proteins in such a bilayer, we would observe these molecules to move apart relatively fast, covering a few nanometers within a few nanoseconds.

Lipid/protein bilayers form closed surfaces in order to avoid hydrophobic edges. In this way, each bilayer membrane defines two compartments, an interior and an exterior one. *In vivo*, these two compartments usually have a complex spatial organization, which implies that any given membrane is typically exposed to different aqueous or macromolecular environments. The membrane molecules can adapt to these different environments by lateral diffusion along the fluid membranes and, in this manner, form distinct membrane segments that differ in their lipid/protein composition. In addition, such compartments can also arise from lateral phase separation and domain formation within the membranes. Whereas ambience-induced segmentation of membranes is governed by the molecular interactions between the membranes and their environments, intramembrane domains arise from the interactions between the different membrane molecules.

The fluidity of the bilayer membranes is also responsible for their remarkable flexibility, which allows them to attain a large variety of different shapes and to undergo a multitude of morphological transformations between these shapes. Thus, whenever we observe such transformations in the optical microscope, i.e., on the micron scale, we obtain direct evidence for the membranes' fluidity on the molecular scale.

About 20 years ago, a systematic comparison between theory and experiment has shown that the polymorphism of lipid bilayers in their fluid state can be understood in terms of a few elastic properties (Berndl et al., 1990; Lipowsky, 1991; Seifert et al., 1991; Miao et al., 1994; Döbereiner et al., 1997). Because the lipids prefer to stay in a state of optimal molecular packing, the membrane area is essentially constant during all shape transformations that do not lead to membrane rupture. These transformations are then governed by bending deformations, which change the membrane curvature and depend primarily on two fluid-elastic parameters (Helfrich, 1973): the membrane's *spontaneous curvature*, which represents the preferred curvature of the membrane and reflects the asymmetry between the two leaflets of the bilayer, and its *bending rigidity*, which describes the resistance of the membrane to bend away from its preferred curvature.

So far, the polymorphism of reconstituted membranes consisting of many lipids and proteins has not been investigated by systematic experimental studies, but from a theoretical point of view, these membranes can again be characterized by their spontaneous curvature and their bending rigidity as long as they remain in a fluid state. *In vivo*, these fluid lipid/protein membranes are often exposed to solid-like structures such as polymerized protein cages or cytoskeletal filaments that exert localized forces onto the membranes. Such forces may also be coupled to active processes involving nucleotide hydrolysis. One example is provided by the concentric patterns of intramembrane domains as observed in the immunological synapse, a pattern that requires active cytoskeletal transport (Weikl and Lipowsky, 2004; Choudhuri and Dustin, 2010). Another example is provided by molecular motors that generate membrane nanotubes from large membranes as observed *in vitro* (Koster et al., 2003; Leduc et al., 2004).

In this paper, I will focus on some simple and generic consequences of membrane fluidity for the remodeling of membrane compartments. The paper is organized as follows. The second section emphasizes the cooperative nature of membrane curvature, explains the precise meaning of this curvature, and introduces the basic fluid-elastic parameters, spontaneous curvature and bending rigidity. The third section describes the generation of spontaneous curvature by asymmetric binding of molecules from the surrounding aqueous compartments. At the end of this section, I consider the binding of BAR-mimetic nanoparticles in order to clarify the distinction between curvature generation and curvature sensing. In the fourth section, another consequence of membrane fluidity is considered: the formation of intramembrane compartments by ambience-induced segmentation and phase separation within the membranes. It is explained that intramembrane domain formation via phase separation should always be confined to single ambience-induced membrane segments. The fifth and sixth sections address the formation of membrane compartments via domain-induced budding and tubulation. For these processes, the size of the new compartments is controlled *locally* by the fluid-elastic properties and the lateral size of the membrane domains. Which of the two processes, budding or tubulation, actually occurs depends on the elastic properties of the domain, on the line tension of the domain boundary, on the adsorption kinetics, and on the presence or absence of external constraints arising, e.g., from the osmotic conditions and adhesive environments. It is also argued that adhering vesicles undergo tubulation when the spontaneous curvature induced by asymmetric adsorption from the two aqueous compartments exceeds a certain threshold value. Experimental methods to actually measure the spontaneous curvature are briefly reviewed in the seventh section, where the recently introduced method based on aqueous two-phase systems is emphasized. The paper concludes with a short summary and outlook.

Qualitative and quantitative aspects of curvature

The cooperative nature of membrane curvature

Curvature is a geometric concept, originally developed by mathematicians to characterize the shape of smooth surfaces. Membranes appear to be rather smooth when viewed in the optical microscope, but this smoothness does *not* persist to molecular scales. Indeed, because membranes are immersed in liquid water, each lipid and protein molecule within the membrane undergoes Brownian motion, which involves displacements both parallel and perpendicular to the membrane. The perpendicular displacements represent molecular protrusions that roughen the two interfaces bounding the membrane (see Figure 1). Therefore, in order to characterize a lipid/protein bilayer by its curvature, one has to consider small membrane patches and average over the molecular conformations within these patches. The minimal lateral size of these patches can be determined from the analysis of molecular dynamics simulations and was found to be about 1.5 times the membrane thickness (see Figure 1) (Goetz et al., 1999). For a lipid bilayer with a thickness of 4 nm, this minimal size is about 6 nm.

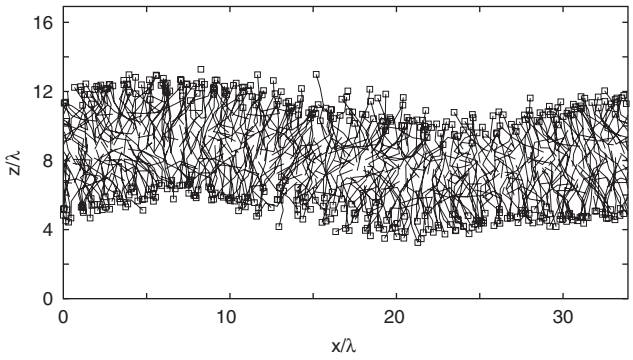

Figure 1 Typical conformation of a lipid bilayer as observed in molecular dynamics simulations. The bilayer has a thickness of about 4 nm and is bounded by two interfaces that are roughened by molecular protrusions, which displace the head groups (open squares) perpendicular to the membrane. In order to characterize such a membrane by its curvature, one has to average over membrane patches with a lateral size that exceeds about 1.5 times the bilayer thickness, as follows from the spectral analysis of the membrane's shape fluctuations (Goetz et al., 1999).

A lipid bilayer patch with a lateral size of 6 nm contains about 80–100 lipid molecules. Therefore, membrane curvature should be viewed as a supramolecular feature arising from the collective behavior of a large number of lipid molecules. The same conclusion applies to the *spontaneous* curvature of membranes as discussed in the following sections.

Symmetric and asymmetric membranes

The lipid bilayer displayed in Figure 1 is symmetric in the sense that it consists of two leaflets that have the same molecular composition and are exposed to the same aqueous solutions on both sides of the membrane. In real systems, such symmetric membranes are somewhat exceptional, but they provide a useful reference system because their elastic properties are governed by a single elastic parameter, the bending rigidity κ that provides the basic energy scale. For phospholipid bilayers, the latter scale is of the order of 10^{-19} J, which is about 20 k_BT at room temperature.

Real membranes are typically asymmetric. This asymmetry may arise from a different lipid composition of the two leaflets as found in all biomembranes. Likewise, membrane proteins in biological membranes have a preferred orientation, which also contributes to the bilayer asymmetry. In addition, membranes can acquire such an asymmetry from their environment as provided by the exterior and interior aqueous compartments. Indeed, the membranes become asymmetric when these two compartments contain different concentrations of ions, small molecules, and/or proteins.

On length scales that exceed the membrane thickness, the asymmetry of the membranes can be described in terms of another elastic parameter, the spontaneous curvature m. It is important to note that this curvature can be positive or negative. In order to define the sign of m in an unambiguous manner, we use the convention that the spontaneous curvature is *positive* if the membrane prefers to bulge toward the *exterior* compartment (see Figure 2A), whereas a membrane with negative spontaneous curvature prefers to bulge toward the interior compartment (see Figure 2C). The intuitive notion of curvature preference was originally discussed in the context of surfactant monolayers by Bancroft and Tucker (1927), included in the curvature elasticity of liquid crystals by Frank (1958), and introduced for lipid bilayers by Helfrich (1973). In order to describe this curvature preference in a quantitative manner, we need to define the membrane curvature in a more precise way, which requires a short excursion into differential geometry.

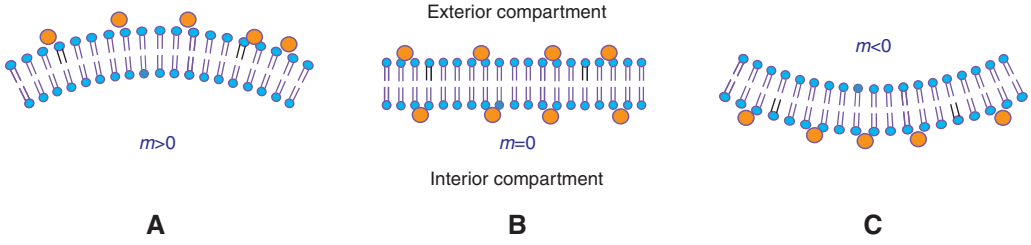

Figure 2 Asymmetric binding of small particles such as ions or small molecules to a membrane generates a spontaneous curvature m in this membrane. The membrane prefers to bulge toward the compartment, that leads to a larger number of adsorbed particles per unit area (Lipowsky and Döbereiner, 1998). It is important to note that the spontaneous curvature m can be positive or negative. In order to define this sign in an unambiguous manner, we use the convention that the spontaneous curvature is *positive* if the membrane prefers to bulge toward the *exterior* compartment as in (A) but negative if it prefers to bulge toward the interior compartment as in (C). If the membrane can actually adapt to the spontaneous curvature, its mean curvature M satisfies $M=m$.

Mathematical excursion: mean curvature *M*

For each point on a smooth surface, we consider the normal vector, i.e., the unit vector perpendicular to the membrane surface, that points toward the exterior compartment. Now, any plane that contains both the chosen point and this normal vector defines a so-called normal section of the membrane surface (see Figure 3A). The intersection between the surface and such a normal section represents a cross-sectional curve through the chosen point with a certain curvature C at this point. We define this curvature to be positive if the cross-sectional curve bulges toward the exterior compartment as in Figure 3A. Now, let us rotate the normal section around the normal vector. As a result of this rotation, the cross-sectional curve through the chosen point changes and so does the curvature C. As we change the rotation angle between 0 and 360°, the latter curvature varies over a certain range as given by $C_{min} \leq C \leq C_{max}$. The two extremal values C_{min} and C_{max} define the so-called principal curvatures at the chosen point.

The two principal curvatures may again be positive and negative, depending on whether the cross-sectional curve bulges toward the exterior or interior compartment (compare Figure 2). Furthermore, any saddle point is characterized by opposite signs of the two principal curvatures.

For fluid membranes as considered here, the molecules diffuse laterally along the membrane, which implies that the membrane surface should be described in terms of geometric quantities that do not depend on the choice of the surface coordinates. Only two such quantities exist, the mean curvature

$$M \equiv \frac{1}{2}(C_{min} + C_{max}) \quad (1)$$

and the Gaussian curvature as given by $C_{min}C_{max}$. In the following, I will focus on shape transformations that do not change the topology of the membranes, which implies that we can ignore the Gaussian curvature (because the area integral over the Gaussian curvature is shape-independent according to the Gauss-Bonnet theorem).

The sign of the mean curvature M depends on the sign of the two principal curvatures C_{min} and C_{max}. If both C_{min} and C_{max} are positive, i.e., if all cross-sectional curves of the membrane bulge toward the exterior compartment, the mean curvature is positive as well. Likewise, the mean curvature M is negative if all cross-sectional curves of the membrane bulge toward the interior compartment. At a saddle point of the membrane surface, where both principal curvatures have opposite signs, the mean curvature M can be positive or negative or even vanish, depending on the relative magnitude of the two principal curvatures.

In general, the principal curvatures and the mean curvature M are local quantities that vary along the membrane surface. Some particularly simple shapes are, however, characterized by constant mean curvature, i.e., all points on the surface have the same mean curvature. Thus, a planar membrane has vanishing mean curvature, M=0, a

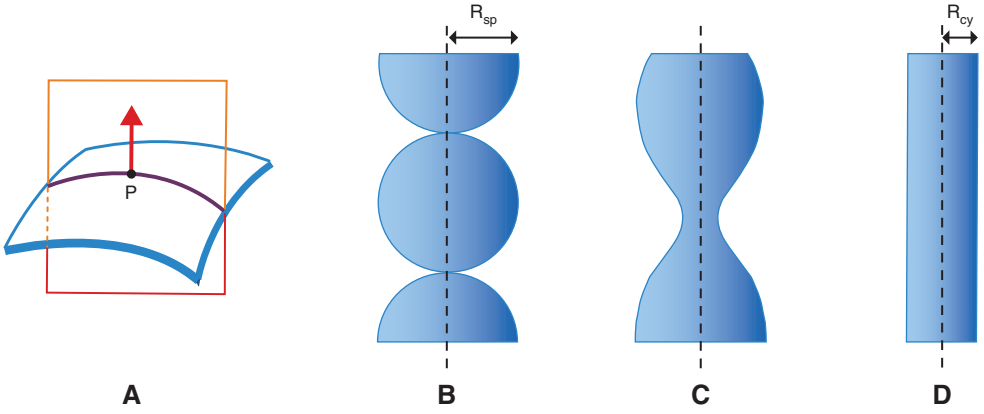

Figure 3 The mean curvature M of the membrane is defined via normal sections as in (A) and attains a constant value for the shapes displayed in (B, C, D): (A) example for a normal section through the membrane surface (blue): consider a small membrane patch represented by point P and the normal vector (red) at P that points toward the exterior compartment. A normal section is provided by any plane that contains both the point P and its normal vector. The intersection between the chosen normal section (orange rectangle) and the membrane surface defines a cross-sectional curve (purple) along the membrane; (B) necklace of spheres with radius R_{sp} and mean curvature $M=1/R_{sp}$; (C) unduloid consisting of lemon-like shapes connected by small necks; and (D) cylinder with radius R_{cy} and mean curvature $M=1/(2R_{cy})$. The shapes are axially symmetric with respect to the broken lines. The radii have been chosen in such a way that all three shapes in (B, C, D) have the same mean curvature M.

sphere with radius R_{sp} has mean curvature $M=\pm 1/R_{sp}$, and a cylinder with radius R_{cy} has mean curvature $M=\pm 1/(2R_{cy})$ (see Figure 3B and D). An unduloid as shown in Figure 3C provides a simple example for a constant mean curvature surface with small necks, which are characterized by two principal curvatures with opposite signs. Biological membranes exhibit such necks during budding and after fusion processes.

Elastic bending energy

The preference of a membrane segment to adapt its mean curvature M locally to the spontaneous curvature m can be described quantitatively by the elastic bending energy

$$\mathcal{E}_{be}=\int dA 2\kappa(M-m)^2, \tag{2}$$

which represents an integral over the area A of the membrane segment.

In the absence of spontaneous curvature, i.e., for $m=0$, the elastic energy as given by (2) has a long history in mathematics. The quadratic expression in the mean curvature was first studied at the beginning of the 19th century by the French mathematician Germain in the context of vibrating plates (Dalmédico, 1991). About a hundred years later, this expression played a prominent role in the work of the German mathematician Blaschke and his students, who were particularly interested in its symmetry properties related to conformal invariance. In the 1960s, the subject was studied in a systematic manner by the British mathematician Willmore, and the shapes that minimize the elastic energy with $m=0$ are now known as Willmore surfaces (Willmore, 1982). As previously mentioned, the notion of a spontaneous curvature m was introduced by Bancroft and Tucker (1927) in the context of surfactant monolayers, such a curvature was included in the elastic splay deformations of liquid crystals by Frank (1958), and the elastic energy for fluid membranes as described by (2) with $m\neq 0$ was first considered by Helfrich (1973).

The elastic bending energy as given by (2) attains its minimal value when the mean curvature M is equal to the spontaneous curvature m everywhere on the membrane surface. The expression (2) also implies that the bending rigidity κ represents a 'spring constant' for deviations of the actual mean curvature M from the spontaneous or preferred curvature m of the membrane.

Real membranes experience a variety of constraints that necessarily lead to such deviations of M from m. One important constraint is provided by the size of the membrane. If its area is large compared to $4\pi/m^2$, the membrane cannot form a single sphere with radius $R_{sp}=1/m$ but could still form a long cylinder with radius $R_{cy}=1/(2m)$. Another important constraint arises from the osmotic conditions that determine the vesicle volume and, thus, the volume-to-area ratio. If the vesicle volume is increased by osmotic inflation, it will eventually attain a spherical shape with mean curvature $M=1/R_{sp}$ that usually differs from the spontaneous curvature m of the vesicle membrane. In fact, for a giant spherical vesicle, the actual mean curvature $M=1/R_{sp}$ can be quite small compared to the spontaneous curvature m and the elastic bending energy of the vesicle membrane is then equal to the membrane area A times the spontaneous tension (Lipowsky, 2013)

$$\sigma\equiv 2\kappa m^2. \tag{3}$$

Such a tension will be present in any membrane segment that has an appreciable spontaneous curvature m but is forced, via external constraints, to assume a mean curvature M that is much smaller than m. Note that κm^2 is the only intrinsic tension scale that can be formed from the two bending-elastic parameters κ and m.

Asymmetric binding of molecules to membranes

A generic mechanism for the generation of spontaneous curvature is provided by exterior and interior compartments that contain different concentrations of 'particles' such as ions, molecules, and nanoparticles. In general, spontaneous curvature can arise both from depletion and from adsorption layers at the two water-membrane surfaces (Lipowsky and Döbereiner, 1998). In order to simplify the discussion, I will focus here on the case of asymmetric adsorption or binding of particles from the two aqueous compartments.

To understand the sign and magnitude of the spontaneous curvature induced by asymmetric binding, it is important to distinguish different size regimes of the particles. Particles are considered to be *small* when their linear size is smaller than the thickness of one bilayer leaflet, i.e., half the membrane thickness; they are considered to be *large* when their linear size exceeds twice the membrane thickness.

Spontaneous curvature induced by ions or small molecules

In vivo, membranes are exposed to aqueous solutions that contain a variety of different ions and small molecules. Likewise, typical *in vitro* assays contain some ions and

small molecules such as glucose as well. These ions and small molecules do not permeate through the bilayers on typical experimental time scales and, thus, determine the osmotic pressures acting on the membranes. In addition, any asymmetry between the concentrations in the exterior and interior compartments generates a spontaneous curvature of the membranes (Lipowsky and Döbereiner, 1998; Lipowsky, 2013).

As a particularly simple example, let us first consider a single molecular species that is adsorbed onto the membrane or, more precisely, onto the head groups of the two leaflets, corresponding to the two water-membrane interfaces bounding the membrane. One example is provided by small amphipathic peptides as studied, e.g., in Ref. (Arouni et al., 2011). Each water-membrane interface can then be characterized by a certain coverage Γ, which is defined by the number of adsorbed particles per unit area. If the peptide concentration in the exterior compartment exceeds the concentration in the interior compartment, the coverage Γ_{ex} of adsorbed peptides on the exterior leaflet exceeds the coverage Γ_{in} on the interior leaflet (see Figure 2A). As long as the membrane surfaces are not saturated with adsorbed peptides, this asymmetric adsorption leads to the spontaneous curvature

$$m=\frac{k_B T}{4\kappa}\ell_{me}(\Gamma_{ex}-\Gamma_{in}) \qquad (4)$$

which depends on the thermal energy $k_B T$, the bending rigidity κ, and the membrane thickness ℓ_{me}. Using typical values for these different parameters, the expression (4) leads to the prediction that the spontaneous curvature m induced by the adsorption of small molecules can be quite large with a maximal value of about 1/(20 nm) (Lipowsky, 2013). The relation (4) between the spontaneous curvature m and the other system parameters has been recently confirmed by coarse-grained molecular dynamics simulations (B. Rózycki and R. Lipowsky (2013). Spontaneous curvature of bilayer membranes from particle-based simulations. *in preparation*).

The derivation of the expression (4) for the adsorption-induced spontaneous curvature m is based on the Gibbs adsorption equation, which contributes the thermal energy $k_B T$ to this expression. Therefore, this simple example nicely illustrates the cooperative nature of the spontaneous curvature. On the other hand, one may also interpret this expression in terms of contributions of single peptides as defined by $m_1=k_B T\ell_{me}/(4\kappa A_{pep})$ where A_{pep} represents the average surface area per adsorbed peptide. The expression (4) can be easily generalized to the adsorption of several molecular species [see (Lipowsky and Döbereiner, 1998)].

The adsorption of ions onto membranes depends, in general, both on the surface charges of the membrane-water interfaces and on the ionic conditions within the aqueous compartments. The presumably simplest case is provided by membranes that are electrically neutral in the absence of ions. If we now add a salt such as KCl to the aqueous solution, the binding of one ionic species, say K^+, to the membrane-water interface necessarily leads to the binding of the other ionic species, in this case Cl^-, as well. Indeed, in such a situation, the second ionic species provides the counterions that ensure electroneutrality of the membrane. These counterions may be directly bound to the membrane-water interface or may form a loosely bound ionic atmosphere in front of this interface. Because the precise spatial organization of the ions does not enter the Gibbs adsorption equation, which represents a thermodynamic relation, the spontaneous curvature m induced by this type of ion adsorption is again described by the expression (4) provided we define the coverages Γ_{ex} and Γ_{in} in an appropriate manner. For a 1:1 electrolyte as provided, e.g., by an aqueous solution of KCl and other alkali metal chlorides (Klasczyk et al., 2010), these coverages are increased by a factor of 2, which reflects the simultaneous binding of ions and counterions.

Spontaneous curvature induced by large molecules

Next, consider large molecules with a size that exceeds twice the membrane thickness, so that it makes sense to characterize the adjacent membrane patches by their curvature. One example is provided by flexible chain molecules such as double-stranded DNA that are anchored to the membrane (see Figure 4A). Another example is given by BAR-domain proteins that adhere to the membranes (see Figure 4B).

The bending of the membrane segment adjacent to such a large molecule increases the elastic bending energy of the membrane. This elastic energy can be balanced by two different mechanisms. In the case of a flexible chain molecule, the bending energy of the membrane is balanced by the entropy of the anchored chain (Lipowsky, 1995). In the case of a BAR-domain protein, the bending energy is balanced by the binding energy between the membrane and the protein.

The two examples in Figure 4A and B also differ in the elastic response of the anchored molecules. A flexible molecule can easily adapt its conformations to the adjacent membrane in order to maximize its configurational entropy. Thus, in this case, both the chain molecule and the membrane will be deformed (Lipowsky, 1995;

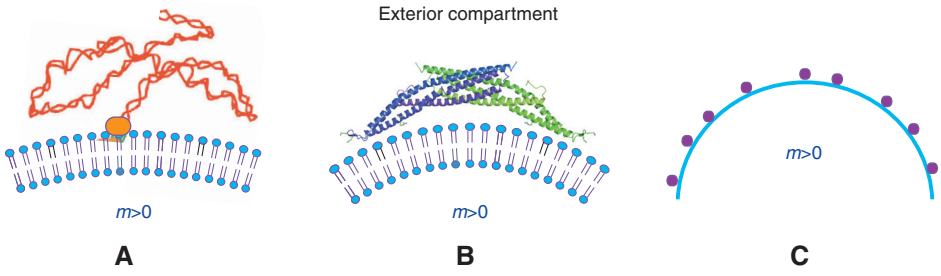

Figure 4 Asymmetric binding of large molecules to membranes: (A) Molecular view of a flexible DNA chain anchored to the membrane (Lipowsky, 1995; Nikolov et al., 2007); (B) molecular view of a BAR-domain protein (Peter et al., 2004; McMahon and Gallop, 2005); and (C) nanoscopic view of a larger membrane segment where the bound 'particles' (purple) may represent flexible chains or BAR-domain proteins. For a spherical segment, the spontaneous curvature m is positive in all three cases. For a spherical segment, the preferred curvature radius in (C) is given by $1/m$.

Breidenich et al., 2000). A BAR-domain protein, on the other hand, is believed to be rather rigid and can then impose its own shape onto the membrane. A whole superfamily of BAR domain proteins has now been identified (Frost et al., 2009); the example in Figure 4B corresponds to the amphiphysin N-BAR protein (Peter et al., 2004; McMahon and Gallop, 2005).

It follows from expression (2) for the elastic bending energy that this energy is small and of the order of a few k_BT for the membrane patches adjacent to the anchored molecules. Thus, in the case of a bound BAR-domain protein, the membrane's bending energy can be easily overcompensated by a few noncovalent bonds between the protein and the membrane.

The banana-like shape of the amphiphysin N-BAR protein shown in Figure 4B has a membrane-binding surface with an area A_{BAR} of about 23 nm^2 and a curvature radius R_{BAR} of about 11 nm (Peter et al., 2004). Now, consider a much larger membrane segment of area A that adsorbs a certain number N_{BAR} of such proteins from the exterior compartment as in Figure 4C. The corresponding protein coverage is given by $\Gamma_{BAR}=N_{BAR}/A$. If the membrane patches between the proteins have a negligible asymmetry, the overall spontaneous curvature of the membrane can be obtained from a superposition of the local membrane curvatures induced by the binding of single BAR domain proteins, in close analogy to the case of anchored chain molecules (Breidenich et al., 2000). Such a superposition leads to the overall spontaneous curvature

$$m=m_{ex}=\frac{A_{BAR}}{2R_{BAR}}\Gamma_{BAR} \quad \text{for} \quad \Gamma_{BAR}<\Gamma_\star \tag{5}$$

where $\Gamma_\star$ represents a critical value of the protein coverage. If the BAR-domain proteins are adsorbed from the interior compartment, the spontaneous curvature would be negative and given by $m=-m_{ex}$. Using the aforementioned values for the area and curvature radius of the amphiphysin N-BAR protein, expression (5) leads to the spontaneous curvature $m\simeq 2.1\ \text{nm}\times\Gamma_{BAR}$. The maximal value of Γ_{BAR} is about $1/A_{BAR}$ or $1/(23\ \text{nm}^2)$. As explained in the next paragraph, the critical coverage $\Gamma_\star$ is about $1/(43\ \text{nm}^2)$, i.e., about half the maximal coverage. Thus, if the exterior leaflet of the bilayer has a coverage Γ_{BAR} of about $1/(100\ \text{nm}^2)$, the resulting spontaneous curvature is about $1/(48\ \text{nm})$.

At the critical coverage $\Gamma_{BAR}=\Gamma_\star$, the adsorbed proteins are expected to undergo an isotropic-nematic transition. Indeed, the curvature superposition underlying the simple expression (5) is only valid as long as the lipid/protein membrane remains in an isotropic liquid state, which implies that the adsorbed BAR domain proteins undergo essentially unrestricted rotational and translational diffusion within the membrane. As the protein coverage is increased, the proteins start to interact with each other and to suppress their rotational degrees of freedom. Because the membrane binding surface of the amphiphysin N-BAR protein has a length of about 14.4 nm and a width of about 1.6 nm, it is characterized by an aspect ratio of about $14.4/1.6\simeq 9$. For hard rods with this aspect ratio, computer simulations (Bates and Frenkel, 2000) lead to the estimate $\Gamma_\star\simeq 4.8/(14.4\ \text{nm})^2\simeq 1/(43\ \text{nm}^2)$ for the critical coverage, which corresponds to about half the maximal coverage. For $\Gamma_{BAR}>\Gamma_\star$, the bound BAR domain proteins will become orientationally ordered, and the spontaneous curvature will no longer be isotropic.

Digression: curvature generation vs. curvature sensing

In the literature on BAR-domain proteins, one often finds the notions of 'curvature generation' and 'curvature sensing'. In order to clarify these notions from a physical point of

view, it is instructive to consider the membrane binding of convex-concave nanoparticles as shown in Figure 5.

In this figure, two types of convex-concave nanoparticles are distinguished depending on their adhesive surface domains that can bind to a membrane. The particle in Figure 5A has a binding domain that extends over the whole concave part of its surface. In contrast, the particle in Figure 5B has a binding domain that is limited to the inner region of the concave surface segment. In both cases, the rest of the particle surface is nonadhesive. Furthermore, both types of nanoparticles are taken to be rigid and, thus, to preserve their shape when they bind to a membrane.

The nanoparticle shown in Figure 5A can bind to a *planar* membrane via the edges of the adhesive surface domain, which correspond to the amphipathic helices of BAR-domain proteins. After the particle and the planar membrane have established these local contacts, the membrane will then spread onto the whole adhesive domain provided by the concave part of the particle surface, a process that necessarily generates membrane curvature. Thus, for a nanoparticle as in Figure 5A, *the membrane can first bind before it curves toward the particle*. The nanoparticle depicted in Figure 5B, on the other hand, cannot bind to a planar membrane but only to a membrane that is already sufficiently curved to reach the adhesive surface domains buried inside the concave part of the particle surface. Thus, in the latter case, *the membrane must first curve before it can bind to the particle*.

In analogy to enzyme-ligand binding, one may consider the curvature generation in Figure 5A as an induced-fit mechanism and the curvature sensing or stabilization in Figure 5B as a mechanism of conformational selection. In this analogy, the nanoparticle (or BAR-domain protein) corresponds to the ligand, the membrane to the enzyme.

Convex-concave nanoparticles similar to those in Figure 5A have been studied in (Reynwar et al., 2007) using simulations of a coarse-grained membrane model with implicit solvent. It was found that, when adsorbed onto a membrane, these particles experience an attractive interaction that can lead to particle aggregation. Even though membrane-mediated interactions between nanoparticles are not considered here, it is interesting to note that attractive, membrane-mediated interactions arise already for spherical nanoparticles that have a chemically uniform adhesive surface (Bahrami et al., 2012). In the latter case, the nanoparticles have a tendency to form linear aggregates enclosed by membrane tubules.

Formation of intramembrane compartments

The membranes considered in the previous sections may contain several lipid and protein components but, so far, have been implicitly assumed to attain a spatially uniform composition. However, when a multicomponent

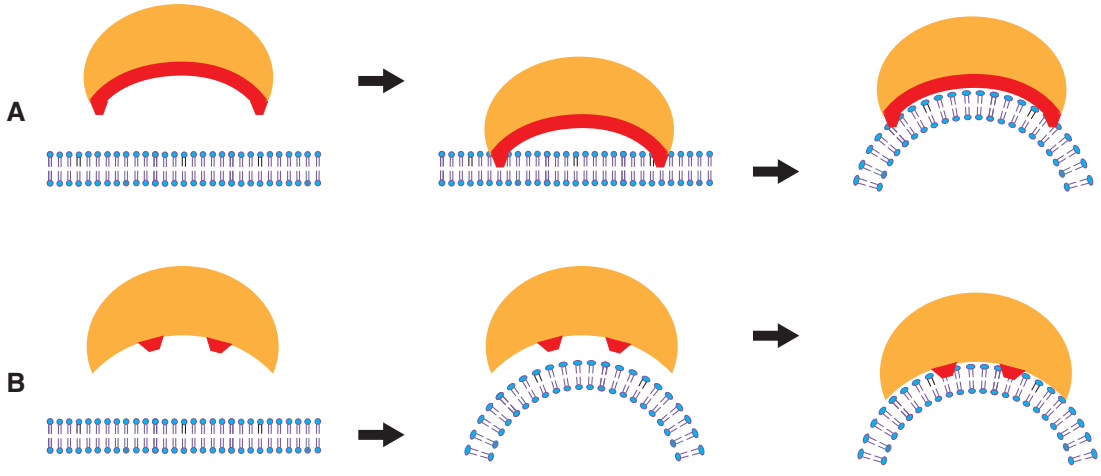

Figure 5 Membrane binding of two types of nanoparticles, which may be considered as BAR-mimetics. The nanoparticles can have the banana-like shape of BAR-domain proteins or, alternatively, the shape of convex-concave lenses. The two types of particles in (A) and (B) differ in the adhesive surface domains (red) that bind to the membrane. In both cases, the rest of the particle surface (orange) is nonadhesive: (A) when the whole concave surface is adhesive, possibly with some reinforcing adhesive structures at the edge, the particle can initially bind to a planar membrane, which subsequently bends to adapt its shape to the concave binding surface; and (B) when the adhesive surface domains are located deep inside the concave part of the particle surface, the membrane must first bend before it can bind to the particle. The process in (A) generates curvature and corresponds to an induced-fit mechanism, whereas the process in (B) stabilizes curvature and represents a mechanism of conformational selection.

membrane is in contact with a nanoparticle or macromolecule as in Figures 5 or 4, these particles and molecules will typically have different affinities for the different membrane components, which implies that the adjacent membrane segments differ in their composition from the rest of the membranes. This ambience-induced enrichment or depletion of membrane molecules is one mechanism for the formation of intramembrane compartments. A second mechanism for the formation of intramembrane compartments is provided by phase separation and domain formation within the membranes. In fact, domain formation via phase separation is affected by the ambience-induced membrane segmentation as discussed in the last subsection below.

Segmentation of membranes by different environments

Some examples for the segmentation of membranes by different environments are displayed in Figure 6. Two relatively simple examples are provided by multicomponent vesicle membranes that adhere to uniform or chemically patterned solid surfaces (see Figure 6A and B). A somewhat more complex geometry is depicted in Figure 6C: three vesicles bounded by membranes that differ in their overall compositions and interact both with the solid support and with other membranes. Furthermore, Figure 6D displays, in a rather simplified manner, the outer cell membrane of a macrophage that moves along a solid surface, contains some cytoskeletal filaments, and engulfs a small particle.

In all cases, the different environments attract the membrane components with different affinities and, thus, have a tendency to recruit certain components to the adjacent membrane segments. In this way, the affinity contrasts between the environments lead to an ambience-induced segmentation of the membranes as illustrated in Figure 6. The examples in Figure 6A, B, and D correspond to single membranes with two, three, and five different membrane segments. The example in Figure 6C depicts three membranes, which are partitioned into three, four, and three segments, respectively. Because of the affinity contrasts between the different environments, each membrane segment will, in general, have a different molecular composition (Lipowsky et al., 2013; Rouhiparkouhi et al., 2013).

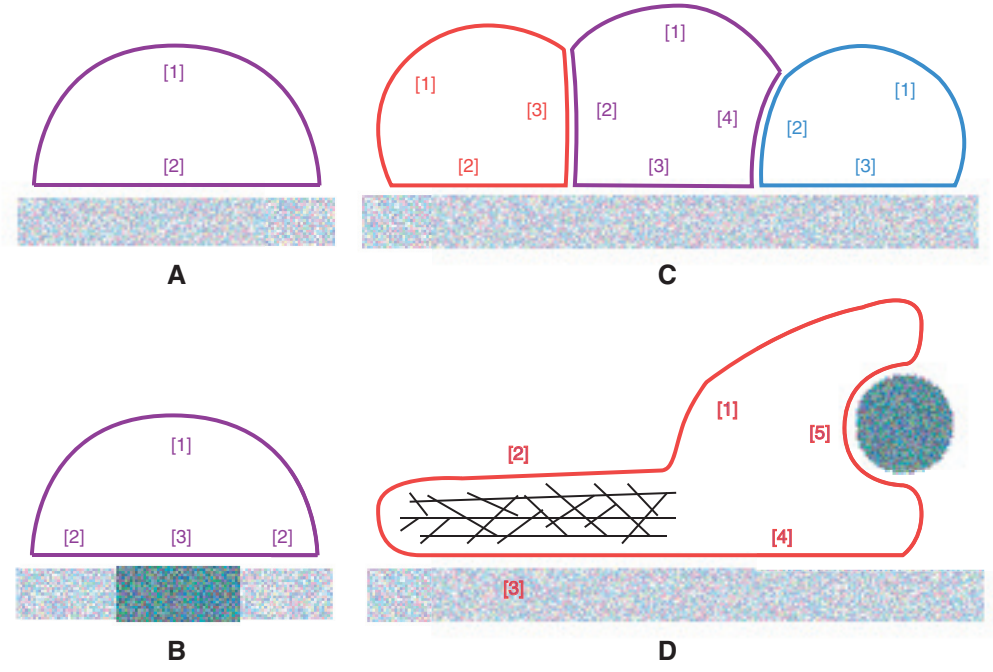

Figure 6 Segmentation of membranes exposed to different environments: (A) vesicle adhering to a uniform surface; (B) vesicle adhering to a chemically patterned surface; (C) cluster of three vesicles adhering to a uniform surface and to each other; and (D) cartoon of a macrophage that moves along a solid surface and engulfs a small particle. The colors of the membranes represent their overall compositions. For each membrane, the numbers [x]=[1], [2], etc., indicate the different ambience-induced membrane segments. Because of the affinity contrasts between the membrane components and the different environments, each membrane segment will, in general, have a molecular composition that differs from the overall composition.

Intramembrane domains arising from phase separation

Because membranes are essentially two-dimensional systems, they can undergo phase separation into different membrane phases. From a biological perspective, the most interesting case corresponds to phase separation into two distinct *fluid* phases, in which the membrane molecules can undergo fast lateral diffusion within all membrane domains (Lipowsky, 1992; Lipowsky and Dimova, 2003). Thus, in the following, we will consider a multicomponent membrane with two types of fluid domains, which differ in their composition. The two intramembrane domains or the corresponding membrane phases will be denoted by *a* and *b*.

The simplest examples for fluid-fluid coexistence in membranes are presumably found in binary mixtures of cholesterol and a single phospholipid. Indeed, spectroscopy methods applied to cholesterol/DMPC (Recktenwald and McConnell, 1981) and cholesterol/DPPC (Vist, 1984; Ipsen et al., 1987; Sankaram and Thompson, 1990; Vist and David, 1990; David et al., 2009) mixtures revealed the formation of two different fluid domains (Marsh, 2010). The interpretation of these domains has been somewhat controversial, however, because it has not been possible, so far, to directly visualize these domains by optical microscopy.

In contrast, direct imaging of domains has been achieved for ternary mixtures consisting of an unsaturated phospholipid, sphingomyelin, and cholesterol, as originally studied in the context of sphingolipid-cholesterol rafts (Simons and Ikonen, 1997). Using fluorescence microscopy, phase separation of ternary mixtures into liquid-ordered and liquid-disordered domains has been studied for a variety of membrane systems including giant vesicles (Dietrich et al., 2001; Baumgart et al., 2003; Veatch and Keller, 2003; Bacia et al., 2005; Dimova et al., 2007; Semrau et al., 2008), solid-supported membranes (Garg et al., 2007; Jensen et al., 2007; Kiessling et al., 2009), hole-spanning (or black lipid) membranes (Collins and Keller, 2008), as well as pore-spanning membranes (Orth et al., 2012). Furthermore, phase separation into liquid-ordered and liquid-disordered domains has also been observed in giant plasma membrane vesicles that contain a wide assortment of lipids and proteins (Baumgart et al., 2007; Veatch et al., 2008).

Domain formation within ambience-induced membrane segments

In contrast to the large intramembrane domains as observed in reconstituted membranes, it has been difficult to directly visualize such domains in biological membranes. This difficulty can be understood if one takes into account that, *in vivo*, these membranes are exposed to rather heterogeneous environments.

Thus, let us again consider membranes that are partitioned into several segments as in Figure 6. As shown in (Lipowsky et al., 2013; Rouhiparkouhi et al., 2013), the affinity contrasts between the different local environments strongly affect the phase behavior of the membranes. First, the affinity contrasts confine the domain formation spatially to single membrane segments. Thus, *domain formation cannot occur simultaneously in more than one segment*. Second, for N_s=2, 3, … different membrane segments, the system exhibits N_s distinct coexistence regions within the composition-temperature plane, e.g., the single coexistence region for the free vesicle membrane is partitioned into N_s nonoverlapping regions. Third, the range of membrane compositions, for which one can observe domain formation in one of the membrane segments, is always *reduced* compared to the composition range of the free membrane. In fact, this reduction becomes more and more pronounced as one increases the number of different environments. Somewhat surprisingly, this confinement of domain formation both in real space and in the phase diagram is predicted to occur even for very small values of the affinity contrasts.

The spatial confinement of domain formation by ambience-induced segmentation is illustrated in Figure 7 for the relatively simple case of vesicles that adhere to a uniform solid surface. In the upper row of this figure, we see freely suspended vesicles with different compositions. The membranes of these vesicles are exposed to a single, uniform environment, corresponding to the two aqueous solutions on both sides of the membranes. In the lower row of Figure 7, we see the same vesicles but now in contact with an adhesive substrate surface that could be provided by a solid substrate or another membrane. For such an adhesion geometry, the membrane consists of two segments that are exposed to two different environments. The unbound membrane segment far away from the surface experiences the same environment and, thus, the same molecular interactions as the free membrane in the absence of the surface. In contrast, the bound membrane segment in close contact with the adhesive surface experiences additional molecular interactions arising from this surface. In the adhering state, phase separation and domain formation can occur either in the bound or in the unbound segment *but not in both segments simultaneously* (Lipowsky et al., 2013; Rouhiparkouhi et al., 2013).

In eukaryotic cells, membranes are typically exposed to a large number of different local environments as provided by other membranes or membrane-bound organelles

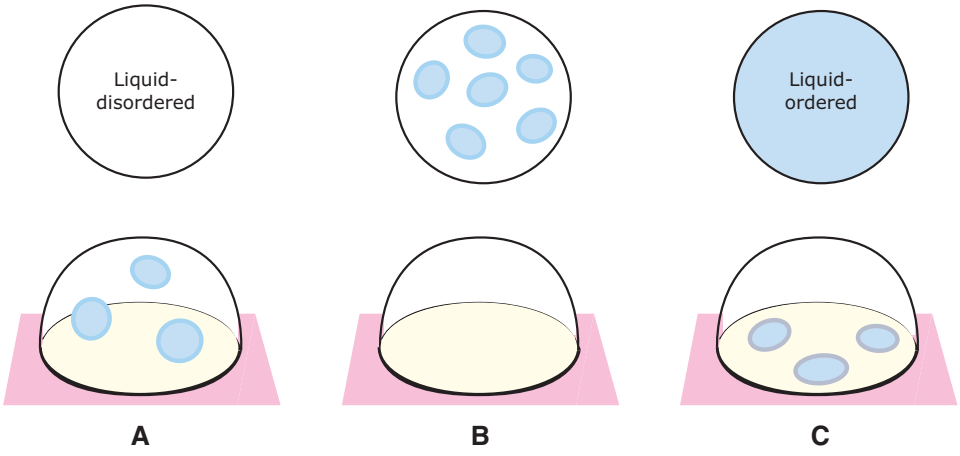

Figure 7 Multicomponent vesicles with three different compositions corresponding to (A) the liquid-disordered phase (white), (B) the two-phase coexistence region, and (C) the liquid-ordered phase (blue). The top row displays the free vesicles, the bottom row the same vesicles now adhering to a rigid surface or solid support. In the adhering state, phase separation and domain formation can occur either in the bound or in the unbound segment *but not in both segments simultaneously* (Lipowsky et al., 2013; Rouhiparkouhi et al., 2013).

as well as by filaments and protein scaffolds (compare Figure 6D). All of these environments will exhibit different molecular affinities for the different membrane components and will, thus, act to suppress domain formation.

Formation of membrane compartments by budding

Intramembrane domains represent two-dimensional compartments, which are connected by lateral diffusion across the domain boundaries. Furthermore, these domains have a tendency to create three-dimensional compartments as well via budding processes as depicted in Figure 8. In fact, a sufficiently large membrane domain consisting of fluid phase b embedded in another fluid phase a must always undergo such a budding process unless the membrane experiences some external constraints that induce a sufficiently large tension (Lipowsky, 1992; Jülicher and Lipowsky, 1993; Kumar et al., 2001; Lipowsky and Dimova, 2003). The different membrane phases a and b are usually characterized by different elastic properties, i.e., by different spontaneous curvatures, m_a and m_b, and different bending rigidities, κ_a and κ_b. In addition, the budding process also depends on the line tension λ of the domain boundaries between the two membrane domains (Lipowsky, 1992).

A b-domain with spontaneous curvature m_b wants to form a spherical cap with radius $R_{bud}=1/m_b$ as indicated in Figure 8A. The direction of budding depends on the sign of the spontaneous curvature m_b of the b-domain: if m_b is positive, the domain forms an out-bud as in Figure 8B; if m_b is negative, it forms an in-bud as in Figure 8C. These b-buds are connected by narrow necks to the large

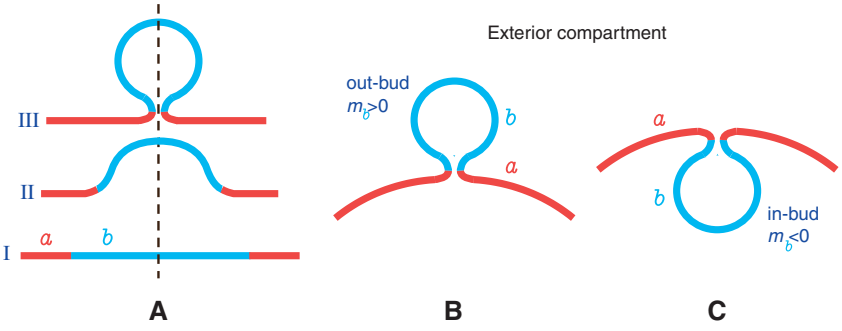

Figure 8 Budding of intramembrane b-domain (blue) within a large, weakly curved a-membrane (red): (A) Starting from the flat state I, the domain forms an incomplete bud, state II, that eventually becomes a complete bud, state III; (B) A *positive* spontaneous curvature of the b-domain leads to out-buds; and (C) A *negative* spontaneous curvature of this domain leads to in-buds. The different states in (A) are axially symmetric with respect to the broken vertical line. Furthermore, the intermediate state II in (A) is a short-lived transient state when the budding process is induced by the line tension of the domain boundary but a long-lived metastable state when this process is driven by an increasing spontaneous curvature.

a-membranes. At first sight, the narrow necks in Figure 8 seem to be highly curved and, thus, to make a large contribution to the elastic energy of the membrane. However, these necks can also adapt their mean curvature M to the spontaneous curvature m. As a consequence, stable membrane necks contribute very little to the elastic energy.

The bud necks provide connections both between the two-dimensional membrane domains and between the three-dimensional water compartments. First, the *b*- and *a*-domains can exchange molecules by lateral diffusion across the membrane segment within the neck. Second, the neck provides a narrow water channel for the exchange of volume between the different water compartments. Thus, the interior compartment of out-buds is connected, via the necks, to the interior compartment of the large mother membrane, whereas the interior compartment of in-buds is connected to the exterior compartment of the large membrane.

Curvature of necks and size of buds

The limit of very narrow (or ideal) membrane necks implies a simple relation between the mean curvatures M_a and M_b of the *a*- and *b*-segments adjacent to this neck. This relation has the form

$$\kappa_a(M_a-m_a)+\kappa_b(M_b-m_b)=\pm\frac{1}{2}\lambda \tag{6}$$

where the plus and minus signs correspond to out- (Jülicher and Lipowsky, 1996) and in-buds (Lipowsky, R. *unpublished*.), respectively. The relation (6) holds if possible differences in the Gaussian curvature moduli of the two domains can be neglected (Jülicher and Lipowsky, 1996).

It is instructive to consider some special cases of the neck condition (6). The simplest case corresponds to a uniform membrane, for which the *a*- and *b*-domains are indistinguishable. In this case, the line tension λ vanishes, and both domains have the same spontaneous curvature $m=m_a=m_b$ as well as the same bending rigidity $\kappa=\kappa_a=\kappa_b$. The neck condition (6) now simplifies and becomes $M_a+M_b=2m$ as obtained in (Seifert et al., 1991; Fourcade et al., 1994). For a weakly curved *a*-segment as in Figure 8, the limit shape of a spherical *b*-bud then has the radius

$$R_{\rm bud}\approx\frac{1}{2|m|}\quad(\text{uniform membrane with weakly curved } a\text{-segment}). \tag{7}$$

Another simple case is provided by a weakly curved *a*-membrane characterized by a small spontaneous curvature $|m_a|\ll|m_b|$. In this case, the *b*-domain forms the limit shape of a spherical bud with radius

$$R_{\rm bud}\approx\frac{1}{|m_b|+\lambda/(2\kappa_b)}\quad(\text{weakly curved } a\text{-membrane with small } |m_a|). \tag{8}$$

Thus, depending on the relative size of the spontaneous curvature $|m_b|$ and the reduced line tension $\lambda/(2\kappa_b)$, the bud size may be dominated by spontaneous curvature or by line tension. For ternary lipid mixtures, the line tension has been measured and was found to be of the order of 10^{-12} N (Baumgart et al., 2005; Semrau et al., 2008). The latter value is about one order of magnitude smaller than simple theoretical estimates because these lipid mixtures are close to a critical demixing point (Lipowsky, 1992). The bending rigidity κ_b has a typical value of the order of 10^{-19} J. Thus, in these systems, the reduced line tension $\lambda/(2\kappa_b)\simeq 1/(200\text{ nm})$, which implies that the bud size is dominated by line tension with $R_{\rm bud}\approx 2\kappa_b/\lambda$ for $|m_b|<1/(200\text{ nm})$ and governed by spontaneous curvature with $R_{\rm bud}\approx 1/|m_b|$ for $|m_b|>1/(200\text{ nm})$.

Dynamics of domain-induced budding

Now, let us address the dynamics of domain-induced budding and consider a circular *b*-domain with area A_b that defines the lateral domain size L_b via $A_b=\pi L_b^2$. Let us further assume that the absolute value $|m_b|$ of the spontaneous curvature is initially small compared to $\lambda/(2\kappa_b)$. In such a situation, the flat or weakly curved state is globally stable if the lateral size L_b is smaller than $4\kappa_b/\lambda$ and remains metastable for $4\kappa_b/\lambda<L_b<8\kappa_b/\lambda$ (Lipowsky, 1992). This metastable state is long-lived because it has to overcome a large energy barrier until the size L_b becomes close to $8\kappa_b/\lambda$. Such a metastable domain can be destabilized by two different dynamical processes: (I) an increase in the domain size for small and constant spontaneous curvature and (II) an increase in the spontaneous curvature for constant domain size.

First, consider process (I), which corresponds to domain growth by lateral phase separation, i.e., by lateral diffusion and segregation of the lipids and proteins within the membrane. Such a growing domain becomes unstable and undergoes domain-induced budding when its lateral size exceeds the value $L_b=8\kappa_b/\lambda$ (Lipowsky, 1992). In this case, the weakly curved and strongly curved state of the membrane domain are initially separated by a large energy barrier, which decreases with increasing domain size and disappears at the critical value $L_b=8\kappa_b/\lambda$. The

corresponding budding process represents an *abrupt or discontinuous* morphological transition from the weakly to the strongly curved state.

On the other hand, for process (II), i.e., when the spontaneous curvature of the domain is increased, e.g., by asymmetric adsorption, for constant domain size L_b, the domain forms a complete bud when the absolute value $|m_b|$ of the spontaneous curvature becomes comparable to $2/L_b$. In the latter case, the energy barrier between the weakly and strongly curved state is small, and domain-induced budding corresponds to a *smooth and essentially continuous* process.

Suppression of domain-induced budding

Domain-induced budding can be suppressed by external constraints. For vesicles, one such constraint arises from the osmotic conditions that determine the vesicle volume. The possibility of budding then depends on the volume-to-area ratio. Osmotic inflation leads to a spherical vesicle with the largest possible volume-to-area ratio. In this case, domain-induced budding is completely suppressed. Likewise, strong adhesion of the vesicles also acts to suppress the budding process. In the latter case, the vesicle forms a spherical cap in order to maximize its contact area with the solid support. It is important to note that, in the presence of such constraints, the *b*-domains remain weakly curved even if they have acquired (i) a large lateral size L_b that may be comparable to the vesicle size and/or (ii) an appreciable spontaneous curvature m_b.

Now, consider such a multidomain vesicle with a *b*-domain that is only weakly curved because of external constraints and let us remove these constraints, e.g., by osmotic deflation. The morphological response of the vesicle now depends on the relative magnitude of the lateral domain size L_b and the inverse spontaneous curvature, $1/m_b$. If L_b is smaller than or comparable to $2/|m_b|$, the *b*-domain undergoes domain-induced budding and forms a partial or complete spherical bud. On the other hand, what happens after the removal of the constraints when the absolute value of the spontaneous curvature is much larger than the inverse domain size and satisfies $|m_b| \gg 2/L_b$? In such a situation, the large *b*-domain could form several spherical buds with radius $R_{bud} \approx 1/(2|m_b|)$ or mean curvature $M_{bud} \approx 2m_b$ as required by the neck condition (7). Each of these buds would have the elastic bending energy $2\pi\kappa_b$, which is identical to the elastic bending energy of the weakly curved membrane segments, from which the buds originated. Therefore, because the mean curvature of the buds is now twice the spontaneous curvature, the *b*-domain *cannot* reduce its elastic bending energy by forming buds of radius $R_{bud}=1/(2|m_b|)$. In contrast, such a reduction is possible if the *b*-domain forms a long nanotube or tubule, the main body of which is characterized by mean curvature $M_{tub}=m_b$ and, thus, by vanishing bending energy, as described in the following section. Therefore, if the spontaneous curvature is much larger than the inverse domain size, the domain will form a long nanotube after the removal of the external constraints.

Another mechanism for the suppression of budding is provided by fast adsorption kinetics. Indeed, it has been implicitly assumed so far that the adsorption-induced increase in the spontaneous curvature is sufficiently slow compared to the budding process, so that the budding domain can always adapt relatively fast to the changing spontaneous curvature. However, if the adsorption is strong and/or if the concentration of the adsorbing particles is high, the adsorption-induced increase in the spontaneous curvature may increase on a time scale that is short compared to the time that the domain needs to form the bud. We then end up with a domain that has typically a large size L_b and, in addition, a large spontaneous curvature $m_b \gg 2/L_b$, i.e., we end up in the same situation that we encountered after the removal of external constraints. Therefore, for fast adsorption kinetics, the *b*-domains will again form long nanotubes.

Spontaneous tubulation of membranes

As discussed in the previous subsection, an intramembrane domain consisting of a lipid or lipid/protein phase *b* can form a long nanotube or tubule if the absolute value of its spontaneous curvature, $|m_b|$, is large compared to its inverse domain size $1/L_b$. Now, let us consider this tubular morphology in more detail and let us distinguish cylindrical from necklace-like nanotubes as shown in Figure 9.

Cylindrical nanotubes

The simplest tubular morphology is provided by a long cylindrical tube as displayed in Figure 9A. When such a *b*-tube protrudes from a larger *a*-membrane, it has the mean curvature (Lipowsky, R. *unpublished*)

$$M_b \approx m_b - \frac{1}{4} M_a \left[\frac{\sigma_a}{\sigma_b} + \frac{\Sigma_a - \Sigma_b}{\sigma_b} \right] \quad \text{for small } M_a \tag{9}$$

corresponding to a weakly curved *a*-membrane with the spontaneous tensions $\sigma_a \equiv 2\kappa_a m_a^2$ and $\sigma_b \equiv 2\kappa_b m_b^2$,

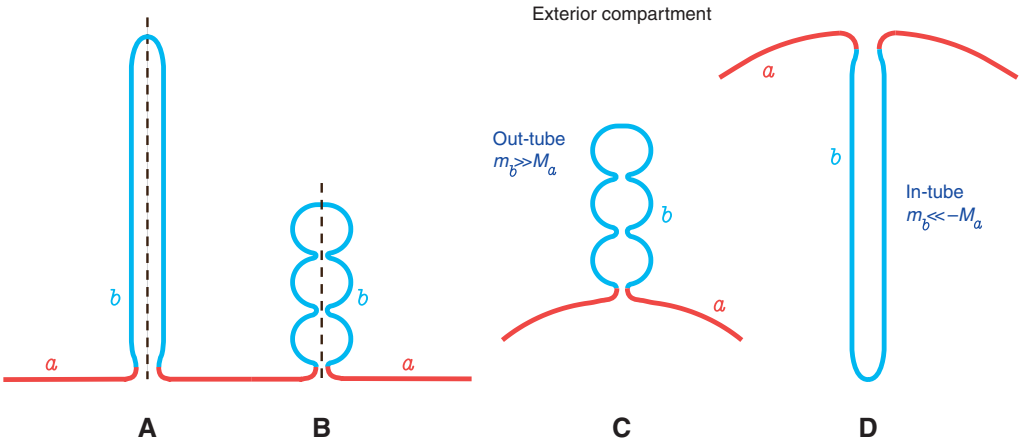

Figure 9 Membrane domains of *b*-phase (blue) within a large membrane segment of phase *a* (red) can form (A) cylindrical nanotubes or (B) necklace-like tubes consisting of a string of small spheres. Both tubes have the same surface area and the same mean curvature M, equal to the domain's spontaneous curvature m_b. The two tubules can be continuously transformed into one another via intermediate unduloids with $M=m_b$ (see Figure 3B); (C) *b*-domains with large positive spontaneous curvature $m_b \gg M_a$ form out-tubes, typically with a necklace-like morphology; and (D) *b*-domains with large negative spontaneous curvature $m_b \ll -M_a$ form in-tubes, which are more likely to have a cylindrical shape. The precise shape of the membrane segment close to the *ab* domain boundary depends on the relative size of the fluid-elastic parameters and may differ from the schematic shape shown here.

compare the definition (3). The correction term in (9) depends on the difference of the mechanical tensions Σ_a and Σ_b that act to stretch or compress the *a* and *b* domains. For a two-domain vesicle with volume V, these tensions follow from

$$\Sigma_i = -\left(\frac{d}{dA_i} E_{\rm be}\right)_{V,A_j} \quad \text{with} \quad i=a,b \quad \text{and} \quad j\neq i, \tag{10}$$

where $E_{\rm be}$ represents the bending energy of the vesicle's equilibrium shape as a function of vesicle volume V and the two domain areas A_a and A_b. The derivative with respect to A_i is taken for constant vesicle volume V and constant domain area A_j. The vesicle volume depends on the osmotic pressure difference acting across the membrane. It is implicitly assumed here that, apart from the osmotic conditions, the vesicle membrane is not subject to other mechanical forces or constraints. In addition, it is also assumed that the mechanical tensions Σ_i are small compared to the tension of rupture, which is typically of the order of a few mN/m.

If the *a* and *b* domains are indistinguishable, they are characterized by identical mean curvatures $m_b=m_a=m$, identical bending rigidities $\kappa_a=\kappa_b=\kappa$, and vanishing line tension $\lambda=0$, which implies both $\sigma_a=\sigma_b$ and $\Sigma_a=\Sigma_b$. In the latter situation, the expression (9) simplifies and becomes $M_b \approx m_b - \frac{1}{4} M_a$ as derived previously in (Li et al., 2011; Lipowsky, 2013).

The mechanical tensions Σ_i as given by (10) depend on the vesicle shape, on the elastic properties of the two membrane domains, and on the line tension. As mentioned, these tensions need to be small compared to the tension of rupture. Furthermore, for lipid membranes, the rupture tensions are, themselves, much smaller than the area compressibility moduli. This separation of tension scales implies that the domain areas A_i are essentially constant during all shape transformations that do not lead to membrane rupture. It is then convenient to consider the domain areas A_i as the basic control parameters and regard the mechanical tensions as Lagrange multipliers (Jülicher and Lipowsky, 1993, 1996). Theoretically, one may also treat the mechanical tensions Σ_i, themselves, as independent control parameters as in (Góźdź and Gompper, 2001; Harden et al., 2005), but the latter approach does not distinguish between different sources of mechanical tension and ignores that the mechanical tensions as given by (10) are determined by the other membrane parameters.

Necklace-like nanotubes

A cylindrical membrane tube may be transformed, for fixed membrane area of the *b*-domain, into a necklace-like tube consisting of a string of small spheres as in Figure 9B. In fact, if the main body of the cylindrical tube has constant mean curvature $M_b=1/(2R_{\rm cy})=m_b$, the necklace-like nanotube has the same constant mean curvature $M_b=m_b$, if the small spheres have the radius $R_{\rm ss}=1/m_b$ as required by the neck condition (6) for two identical membrane

segments. Thus, both the cylindrical and the necklace-like nanotube can adapt their mean curvature to the spontaneous curvature m_b of the b-membrane, which implies that the elastic bending energy vanishes for the main body of both tubes. In fact, the transformation from the cylindrical to the necklace-like tube can proceed in a continuous manner via unduloids (see Figure 3C), which are also constant mean curvature surfaces with $M_b=m_b$ and, thus, characterized by vanishing elastic bending energy (apart from the two ends of the tubes).

In this way, one is led to consider a continuous transformation from the cylindrical to the necklace-like tube. This transformation is characterized by constant membrane area, constant mean curvature $M=m_b$, and vanishing elastic energy of the main tube body but involves a reduction in the tube length by a factor 1/2 and an increase in the tube volume by a factor 4/3 (Lipowsky, 2013). Therefore, this transformation leads to positive or negative volume work depending on the osmotic pressure difference experienced by the tube membrane. As a result, one finds that necklace-like out-tubes as in Figure 9C have a lower free energy than cylindrical out-tubes, whereas cylindrical in-tubes as in Figure 9D have a lower free energy than necklace-like in-tubes.

For a cylindrical tubule of length L_{cy} connected to a weakly curved a-membrane with small mean curvature M_a, the free energy difference between the cylindrical and the necklace-like tube is given by $\mp(\pi/3)c_\sigma\kappa_b L_{cy}M_a$ with $c_\sigma\equiv(\sigma_a+\Sigma_a-\Sigma_b)/\sigma_b$, where the minus and plus sign corresponds to out- and in-tubes, respectively. This free energy difference is of the order of few k_BT or smaller if the vesicle size $1/M_a$ is large compared to the tube length L_{cy}, and the dimensionless coefficient c_σ is of the order of 1. One then expects to see peristaltic shape fluctuations or 'soft modes' between the cylindrical and the necklace-like tube. For long tubes with L_{cy} comparable to the vesicle size $1/M_a$, on the other hand, the free energy difference is of the order of the bending rigidity κ and, thus, about 20 k_BT for $c_\sigma\simeq1$. In the latter case, one expects to see only small peristaltic fluctuations around the tube with the lower free energy.

Competition between tubulation and adhesion

In the previous subsections, we considered a membrane segment with two domains, a and b, and explored the possibility that the b-domain forms a cylindrical or necklace-like nanotube without paying attention to external constraints acting on the whole vesicle. If this membrane segment belongs to a large vesicle, tubulation is only possible if the whole vesicle can change its morphology in an appropriate manner. A simple example for an external constraint that acts to suppress tubulation is provided by a vesicle adhering strongly to another surface as depicted in Figure 10A.

If the adhesive strength $|W|$ of this surface, which represent the adhesion energy per unit area, exceeds the energy density $\kappa/(0.5\ \mu m^2)$ corresponding to a value of about 10^{-4} mN/m for lipid bilayers, the contact curvature of the adhering membrane is below optical resolution, and the vesicle appears to have the shape of a spherical cap (Seifert and Lipowsky, 1990). The effective contact angle of this cap reflects the volume-to-area ratio of the vesicle. Thus, let us consider such a strongly adhering

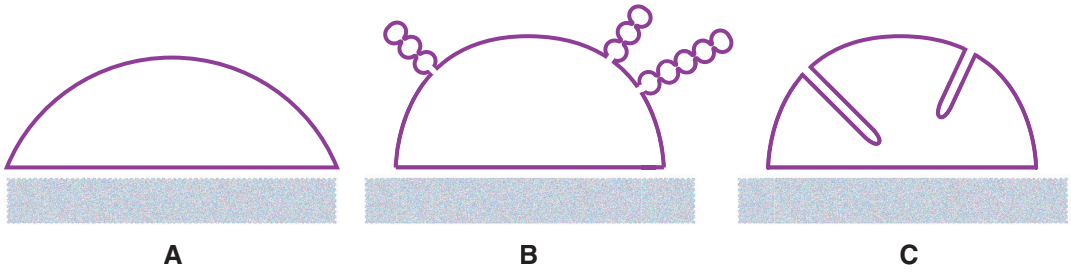

Figure 10 Vesicles adhering to a solid surface: (A) If the vesicle membrane has a small spontaneous curvature, the strongly adhering vesicle forms a spherical cap, the geometry of which reflects its volume-to-area ratio; (B, C) Membrane binding of proteins or nanoparticles that generate a large positive or negative spontaneous curvature m: if the absolute value $|m|$ exceeds a certain threshold value, the vesicle starts to reduce its contact area with the solid surface and store the resulting excess area in necklace-like out-tubes for $m>0$ as in (B) and in cylindrical in-tubes for $m<0$ as in (C). In both cases, the tubulation process will continue until the contact area disappears and the vesicle unbinds from the solid surface. In addition to the straight tube conformations shown here, the nanotubes can attain many curved and undulating conformations as a result of thermally excited shape fluctuations. Furthermore, peristaltic shape fluctuations of the cylindrical tubes lead to necklace-like morphologies.

vesicle and assume that it is initially characterized by a relatively small spontaneous curvature as in Figure 10A. More precisely, we consider a membrane with a uniform composition and with a spontaneous curvature m that is initially small compared to the mean curvature of the spherical cap.

Now, let us assume that the exterior or the interior compartment contains some proteins or nanoparticles that adsorb onto the vesicle membrane and act to increase the spontaneous curvature m of the membrane. For the molecules and nanoparticles previously depicted in Figures 4 and 5, the spontaneous curvature is positive and negative if these particles adsorb from the exterior and interior compartment, respectively. In addition, it is not difficult to envisage other types of particles that induce the opposite spontaneous curvature. One example is provided by small spherical Janus particles that adhere to the membrane only via their 'south poles'.

As the spontaneous curvature grows via asymmetric adsorption, the membrane would prefer to curve more strongly and to form necklace-like out-tubes as in Figure 10B or cylindrical in-tubes as in Figure 10C. Inspection of these morphologies reveals, however, that these tubes can only form if the contact area between the solid surface and the membrane shrinks, which implies that the membrane loses adhesion energy. Thus, the vesicle morphology now depends on the competition between tubulation and adhesion.

If the particles are adsorbed from the interior compartment of the vesicle, tubulation is energetically favorable if the absolute value of the spontaneous curvature, $|m|$, exceeds a certain threshold, m_*, and satisfies

$$|m|>m_* \equiv \sqrt{|W|/(2\kappa)} \tag{11}$$

as follows from the balance between bending and adhesion energy for a small membrane segment within the contact area of the vesicle membrane. Note that the threshold value m_* for the spontaneous tension is equivalent to the threshold value $\sigma_*=|W|$ for the spontaneous tension σ as defined in (3). The same threshold values apply to particle adsorption onto solid-supported bilayers from aqueous bulk phases (Lipowsky, 2013).

Likewise, for the adhering vesicle, the same threshold value $m_*=\sqrt{|W|/(2\kappa)}$ is also found for particle adsorption from the exterior compartment of the vesicle provided the particles are sufficiently small and can enter the water gap within the contact area. If the particles are large and cannot enter this gap, tubulation is only favorable if the initial vesicle has a sufficiently small contact angle and, thus, a sufficiently small volume-to-area ratio.

In order to start from a spherical cap shape as in Figure 10A, the adhesion energy density $|W|$ has to be larger than 10^{-4} mN/m. Using the latter value for $|W|$ together with the value $\kappa \simeq 10^{-19}$ J for lipid bilayers, we find that the threshold value m_* is about 1/(μm). When we compare this threshold value with the spontaneous curvatures m as generated by asymmetric adsorption of small or large molecules, see relations (4) and (5) above, we conclude that such an adsorption-induced spontaneous curvature can certainly exceed the threshold value $m_* \simeq 1/(\mu m)$.

Once the spontaneous curvature exceeds its threshold value m_*, the vesicle can reduce its combined elastic and adhesive energy by forming nanotubes with a mean curvature $M_{tub}=m$. After one or a few nanotubes have been nucleated as in Figure 10B and C, they will continue to grow until the contact area of the vesicle disappears completely and the vesicle unbinds from the solid surface. In this way, the generation of a sufficiently large spontaneous curvature $m>m_*$ should lead to the unbinding of adhering vesicles.

Spontaneous vs. force-induced tubulation

It has been known for some time that membrane tubules or nanotubes, often denoted as 'tethers', can be pulled from large vesicles by applying external forces to the membranes (Bo and Waugh, 1989; Hochmuth et al., 1996; Sorre et al., 2012; Zhu et al., 2012). It is less obvious that such tubules may also form spontaneously, i.e., in the absence of external forces. Nevertheless, spontaneous tubulation has been observed for a variety of systems. Indeed, many different proteins have been identified that adsorb onto liposomes and lead to extended membrane tubules. These proteins include N-BAR proteins such as amphiphysin (Takei et al., 1999; Peter et al., 2004) and endophilin (Farsad et al., 2001), F-BAR proteins such as syndapins (Wang et al., 2009), and other proteins involved in endocytosis such as epsin (Ford et al., 2002).

Very recently, two different *unilamellar* systems have been observed to undergo spontaneous tubulation. One of these systems is provided by supported lipid bilayers that were exposed to a variety of antimicrobial peptides (Domanov and Kinnunen, 2006; Mally et al., 2007; Domingues et al., 2010; Arouni et al., 2011). It has been argued in (Lipowsky, 2013) that these supported bilayers provide an example for the competition between adhesion and tubulation via spontaneous curvature. The other system consists of giant vesicles in contact with aqueous solutions of PEG and dextran, which undergo phase separation into PEG-rich and dextran-rich droplets (Li et al.,

2011; Dimova and Lipowsky, 2012). The latter system turns out to provide a novel method to measure the spontaneous curvature as explained in the following section.

Measuring the spontaneous curvature

In all previous sections, the spontaneous curvature of membranes played a prominent role. This curvature has been estimated theoretically for a variety of systems. Up to recently, these estimates have been hardly scrutinized by experiment, however, because the available experimental methods have been rather limited.

Limitations of previous experimental methods

Presumably the first attempts to measure the spontaneous curvature of lipid bilayers was based on 'flicker spectroscopy', i.e., the spectral analysis of shape fluctuations of quasi-spherical vesicles as observed in the optical microscope. One example is provided by lipid bilayers exposed to a mixture of two sugar molecules, the monosaccharide glucose and the trisaccharide raffinose [see (Döbereiner et al., 1999)]. Using flicker spectroscopy, the spontaneous curvature was found to vary from about 0.01/μm–0.1/μm, comparable to or somewhat larger than the mean curvature of the vesicle membranes. These experimental values agreed with theoretical estimates based on two depletion layers in front of the two membrane surfaces (Lipowsky and Döbereiner, 1998). Much larger values of the spontaneous curvature m are hardly accessible to the experimental method of flicker spectroscopy because the vesicle membrane then tries to form highly curved segments in the form of nanotubes, whereas the weakly curved segments experience a large spontaneous tension $\sigma=2\kappa m^2$ that acts to suppress the flickering (Lipowsky, 2013). Indeed, the largest m-values that have been determined by this method are about five times the inverse vesicle radius (Döbereiner et al., 2003).

Another experimental approach that can be used to determine the spontaneous curvature of membranes is based on the budding of vesicles. When the bud is connected to the mother vesicle by a narrow neck, the mean curvatures M_a and M_b of the membrane segments adjacent to the neck satisfy the neck condition $M_a+M_b\leq 2m$ for an out-bud. This method has been applied to biotinylated DNA bound to membrane-anchored avidin (Nikolov et al., 2007). For the latter system, the spontaneous curvature deduced from vesicle budding was found to lie between 0.1/μm and 1/μm. The method involves a large statistical error, however, because it is often difficult to determine the precise values of the mean curvatures M_a and M_b for a sufficiently large sample of vesicles.

Spontaneous curvature from contact angles

It has been recently shown that the spontaneous curvature of membranes can be measured using large vesicles that enclose two liquid droplets consisting of two different aqueous phases (Li et al., 2011; Dimova and Lipowsky, 2012; Lipowsky, 2013). The aqueous two-phase systems studied, so far, consisted of solutions of PEG and dextran. These solutions form a uniform aqueous phase at sufficiently low polymer concentrations and undergo phase separation into two aqueous phases, a PEG-rich and a dextran-rich phase, when one increases these concentrations above a few weight percent.

The vesicles are initially prepared in such a way that their interior compartments contain a uniform polymer solution. The volume of the vesicle is then reduced by increasing the osmolarity of the aqueous solution in the exterior compartment. As a result of this osmotic deflation, the polymer concentration within the interior compartment of the vesicle increases, and the solution then undergoes phase separation into two liquid droplets. The resulting vesicle morphology is displayed in Figure 11A where the PEG-rich phase is denoted by α and the dextran-rich phase by β. The composition of the exterior aqueous compartment, which is, in general, different from the composition of the α and β phases, is denoted by γ.

The morphology shown in Figure 11A involves three different surfaces. First, the two liquid droplets α and β are separated by a liquid-liquid interface. Second, because the membrane is in contact with different aqueous phases, it is partitioned into two segments, an $\alpha\gamma$ segment between the PEG-rich droplet and the exterior solution and a $\beta\gamma$ segment between the dextran-rich droplet and the exterior medium. Both membrane segments are observed to form spherical caps, which implies that they experience appreciable tensions. The $\alpha\beta$ interface and the two membrane segments meet along the contact line, where they define the three effective contact angles θ_α, θ_β, and θ_γ as shown in Figure 11A and B. These angles can be directly measured in the optical microscope and are related to the tensions of the interface and the two membrane segments. The effective contact angles depend on the vesicle geometry

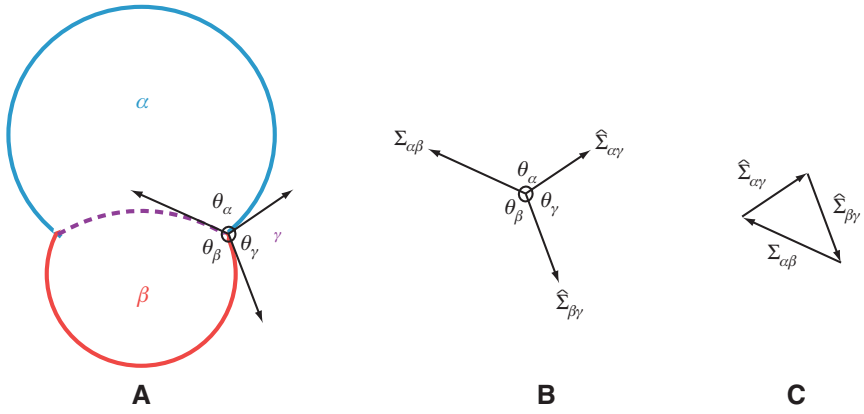

Figure 11 Geometry of a large vesicle enclosing two droplets of distinct aqueous phases: (A) The vesicle membrane separates the two interior aqueous phases α and β from the exterior aqueous phase γ. This membrane consists of two spherical segments, one segment (blue) in contact with the α phase and another segment (red) in contact with the β phase. The $\alpha\beta$ interface (broken line) and the two membrane segments meet along the contact line, which defines the three effective contact angles θ_α, θ_β, and θ_γ; (B) mechanical equilibrium at the contact line implies that the interfacial tension $\Sigma_{\alpha\beta}$ balances the two membrane tensions $\hat{\Sigma}_{\alpha\gamma}$ and $\hat{\Sigma}_{\beta\gamma}$; and (C) triangle formed by the three tensions $\Sigma_{\alpha\beta}$, $\hat{\Sigma}_{\alpha\gamma}$, and $\hat{\Sigma}_{\beta\gamma}$.

and, in particular, on the volumes of the two liquid droplets. Because the membranes must be smoothly curved on nanoscopic scales, the system also involves an intrinsic contact angle θ_{in} that represents a material parameter and can be expressed in terms of the effective contact angles (Kusumaatmaja et al., 2009).

The $\alpha\beta$ interface is characterized by the interfacial tension $\Sigma_{\alpha\beta}$, whereas the two membrane segments experience the membrane tensions $\hat{\Sigma}_{\alpha\gamma}$ and $\hat{\Sigma}_{\beta\gamma}$ (see Figure 11B), which can be decomposed according to (Li et al., 2011; Lipowsky, 2013)

$$\hat{\Sigma}_{\alpha\gamma}=\Sigma_{\alpha\gamma}+\sigma_{\alpha\gamma}=\Sigma_{\alpha\gamma}+2\kappa_{\alpha\gamma}m_{\alpha\gamma}^2 \tag{12}$$

and

$$\hat{\Sigma}_{\beta\gamma}=\Sigma_{\beta\gamma}+\sigma_{\beta\gamma}=\Sigma_{\beta\gamma}+2\kappa_{\beta\gamma}m_{\beta\gamma}^2 \tag{13}$$

where the first and the second terms represent the mechanical and the spontaneous tensions, respectively. In general, the two mechanical tensions $\Sigma_{\alpha\gamma}$ and $\Sigma_{\beta\gamma}$ may have different values [see online 'Additions and Corrections' to (Lipowsky, 2013)]. Furthermore, the spontaneous tensions $\sigma_{\alpha\gamma}$ and $\sigma_{\beta\gamma}$ can dominate the membrane tensions if the spontaneous curvatures $m_{\alpha\gamma}$ and $m_{\beta\gamma}$ are sufficiently large.

The latter situation applies to lipid membranes in contact with PEG-dextran mixtures. For this system, the $\alpha\gamma$ membrane segments are found to form both highly curved nanotubes and weakly curved spherical membrane caps, which implies (i) that the spontaneous curvature $m_{\alpha\gamma}$ is large compared to the mean curvature $M_{\alpha\gamma}$ of the large spherical $_{\alpha\gamma}$ caps and (ii) that the spontaneous tension $\sigma_{\alpha\gamma}$ is large compared to the mechanical tension $\Sigma_{\alpha\gamma}$. As a consequence, the spontaneous curvature $m_{\alpha\gamma}$ can be obtained from

$$m_{\alpha\gamma}\approx-\left[\frac{\hat{\Sigma}_{\alpha\gamma}}{2\kappa_{\alpha\gamma}}\right]^{1/2}=-\left[\frac{\Sigma_{\alpha\beta}}{2\kappa_{\alpha\gamma}}\frac{\sin\theta_\beta}{\sin\theta_\gamma}\right]^{1/2} \tag{14}$$

where the negative sign follows from the observation that the nanotubes always point toward the vesicle interior. Using the relation (14), one finds that the spontaneous curvature $m_{\alpha\gamma}$ is about -1/(240 nm) for a certain concentration of PEG and dextran. The relation (14) has recently been confirmed by directly measuring the diameter of the tubes (Liu, Y., Kusumaatmaja, H., Dimova, R., and Lipowsky, R. (2013). Lipid membranes exposed to asymmetric environments acquire spontaneous tensions. *in preparation*).

The three tensions must balance along the contact line (see Figure 11B and C). The corresponding force balance equation has the general form

$$\hat{\Sigma}_{\beta\gamma}=\hat{\Sigma}_{\alpha\gamma}+\Sigma_{\alpha\beta}\frac{\sin\theta_\alpha-\sin\theta_\beta}{\sin\theta_\gamma}=\hat{\Sigma}_{\alpha\gamma}+\Sigma_{\alpha\beta}\cos\theta_{\text{in}} \tag{15}$$

For lipid vesicles in contact with the PEG-dextran mixture, the formation of the nanotubes implies that the membrane tension $\hat{\Sigma}_{\alpha\gamma}$ is dominated by the spontaneous tension $\sigma_{\alpha\gamma}$. The force balance equation then simplifies and becomes

$$\hat{\Sigma}_{\beta\gamma}\approx\sigma_{\alpha\gamma}+\Sigma_{\alpha\beta}\cos\theta_{\text{in}}=2\kappa_{\alpha\gamma}m_{\alpha\gamma}^2+\Sigma_{\alpha\beta}\cos\theta_{\text{in}}. \tag{16}$$

It it interesting to note that all parameters that appear on the right-hand side of this equation are material parameters that do not depend on the vesicle geometry.

Summary and outlook

In this paper, a few simple and generic consequences of membrane fluidity have been discussed. First, fluidity implies unusual elastic properties that involve primarily two fluid-elastic parameters, the spontaneous curvature m and the bending rigidity κ. In order to define these parameters, one has to smoothen the molecular roughness of the bilayers (see Figure 1) and average over bilayer patches with a lateral size that is somewhat larger than the bilayer thickness. These bilayer patches contain between 80 and 100 lipid molecules, which directly reveals the cooperative nature of membrane curvature.

One generic mechanism for the generation of spontaneous curvature is provided by the asymmetric adsorption of 'particles' such as ions, small molecules, proteins, or nanoparticles from the surrounding aqueous compartments. Even ions can lead to an appreciable spontaneous curvature m as predicted by the expression (4), which depends on the particle coverage on the two leaflets of the bilayer and leads to a maximal spontaneous curvature value of about 1/(20 nm) (Lipowsky and Döbereiner, 1998; Lipowsky, 2013). Interestingly, the latter value is comparable to the maximal spontaneous curvature (5) that adsorbed BAR-domains can generate in their isotropic fluid state. Such a fluid state should apply up to the critical coverage $\Gamma_* \simeq 1/(43\ \mathrm{nm}^2)$ as estimated from the isotropic-nematic transition for hard rods.

In the subsection on *Curvature generation versus curvation sensing*, the asymmetric binding of convex-concave nanoparticles has been discussed, which mimic the binding of BAR-domain proteins (see Figure 5). Two different types of such BAR-mimetics were considered. For the nanoparticle displayed in Figure 5A, membrane and particle can bind before the membrane curves toward the particle. In analogy to enzyme-ligand binding, this process of curvature generation can be regarded as an induced-fit mechanism. For the particle in Figure 5B, on the other hand, the membrane must first curve before it can bind to the particle. This latter process of curvature sensing or stabilization corresponds to a conformational selection mechanism.

Another interesting consequence of membrane fluidity is the formation of intramembrane compartments that may arise via ambience-induced membrane segmentation (see Figure 6) or via phase separation within the membranes. Theoretical studies predict (Lipowsky et al., 2013; Rouhiparkouhi et al., 2013) that intramembrane domains arising from phase separation are always confined to a single ambience-induced membrane segment (see Figure 7). This interplay between ambience-induced segmentation and domain formation via phase separation provides a simple and generic explanation for the difficulty to observe phase domains *in vivo* (see Figure 6D).

New compartments can be formed by domain-induced budding and tubulation (see Figures 8 and 9). For these processes, the size of the new compartments is controlled *locally* by the elastic properties and the lateral size of the domains. In general, three fluid-elastic parameters determine the size of the new compartments: the spontaneous curvature m_b and the bending rigidity κ_b of the domain as well as the line tension λ of the domain boundary. In order to disentangle the influence of these different parameters, two different types of dynamical processes have been explicitly discussed. In process (I), the domain size grows via lateral diffusion within the membranes, while its spontaneous curvature remains small during the whole process. In process (II), the domain has a constant lateral size, but its spontaneous curvature increases with time, e.g., by adsorption of proteins from the exterior or interior aqueous compartments.

If we ignore possible external constraints, process (I) leads to an abrupt and discontinuous budding transformation of the domain as soon as the domain size L_b has reached the critical size $8\kappa_b/\lambda$ (Lipowsky, 1992). Using typical values for the fluid-elastic parameters of lipid bilayers, this critical size is of the order of 1 μm. For such an unconstrained membrane, process (II) leads to a smooth and essentially continuous budding process provided the adsorption kinetics is sufficiently slow. External constraints as well as fast adsorption kinetics can lead to b-domains that have an initial domain size $L_b \gg 2/|m_b|$. In the latter case, each b-domain could form many spherical buds, but these buds would have a mean curvature that is twice the spontaneous curvature m_b, which implies that the formation of these buds does not reduce the bending energy of the domain. Therefore, the large b-domain will form long nanotubes or tubules as shown in Figure 9.

An interesting example for the interplay between an external constraint acting on the membrane and tubulation is provided by adhering vesicles as depicted in Figure 10. If such a vesicle is exposed to asymmetric adsorption leading to an increasing spontaneous curvature, the vesicle is predicted to unbind from the adhesive surface via spontaneous tubulation as soon as the spontaneous curvature has reached a certain threshold value m_*, which

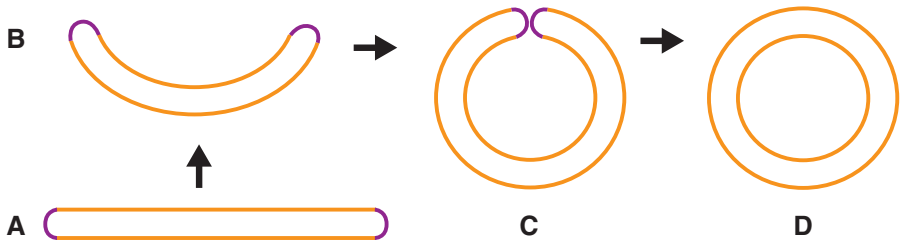

Figure 12 Possible mechanism for shape transformations during autophagocytosis: initially, the vesicle membrane (orange-purple line) has the shape of a double-membrane disk state (A) that closes up via the cup-shape morphology in state (B) to form a double-membrane vesicle as in state (D). The curvature is generated by the elastic bending energy of the strongly curved membrane segment (purple) that acts as an effective rim tension for the double-membrane disk. In state (C), the two spherical membranes are still connected by a small membrane neck, which then undergoes fission to form state (D) (Knorr et al., 2012).

depends only on the bending rigidity and on the adhesive strength of the surface [see equation (11)].

Finally, it was pointed out that the theoretical estimates for the spontaneous curvature as described in the section on *Asymmetric binding of molecules to membranes* have been hardly scrutinized by experiment because the available experimental methods to actually measure the spontaneous curvature were quite limited for a long time. This situation has changed recently with the advent of a novel method based on aqueous two-phase systems (see Figure 11). This method can be further improved by developing suitable reference systems, which allow us to measure changes in spontaneous curvature as induced by single molecular species.

As a short outlook, let me briefly mention another shape transformation of biological membranes that can again be understood in terms of the membranes' fluid elasticity. Many organelles are enclosed by double membranes, i.e., by two lipid/protein membranes that are separated by a thin water layer. The initial morphology of these double-membrane organelles often corresponds to a double-membrane disk, i.e., an essentially flat pancake-like shape, which consists of two apposing bilayers connected by a strongly curved rim (see Figure 12A). These double-membrane sheets grow in lateral size and then close up to form a double-membrane vesicle. One example for such closure processes is provided by autophagocytosis, a membrane-mediated intracellular degradation process. We have recently proposed a relatively simple mechanism for this generation of membrane curvature as depicted in Figure 12 (Knorr et al., 2012). This mechanism is primarily based on the spontaneous curvature of the rim of the double-membrane disk, which may be controlled by the adsorption or desorption of proteins.

Acknowledgments: The view described here has evolved over many years. I would like to thank all my collaborators and, in particular, Rumiana Dimova and Thomas Weikl for enjoyable and fruitful interactions.

Received August 26, 2013; accepted November 30, 2013

References

Arouni, A., Kiessling, V., Tamm, L., Dathe, M., and Blume, A. (2011). Morphological changes induced by the action of antimicrobial peptides on supported lipid bilayers. J. Phys. Chem. *115*, 158–167.

Bacia, K., Schwille, P., and Kurzchalia, T. (2005). Sterol structure determines the separation of phases and the curvature of the liquid-ordered phase in model membranes. PNAS *102*, 3272–3277.

Bahrami, A.H., Lipowsky, R., and Weikl, T.R. (2012). Tubulation and aggregation of spherical nanoparticles adsorbed on vesicles. Phys. Rev. Lett. *109*, 188102.

Bancroft, W. and Tucker, C. (1927). Gibbs on emulsification. J. Phys. Chem. *31*, 1681–1692.

Bates, M.A. and Frenkel, D. (2000). Phase behavior of two-dimensional hard rod fluids. J. Chem. Phys. *112*, 10034–10041.

Baumgart, T., Hess, S., and Webb, W. (2003). Imaging coexisting fluid domains in biomembrane models coupling curvature and line tension. Nature *425*, 821–824.

Baumgart, T., Das, S., Webb, W.W., and Jenkins, J.T. (2005). Membrane elasticity in giant vesicles with fluid phase coexistence. Biophys. J. *89*, 1067–1080.

Baumgart, T., Hammond, A.T., Sengupta, P., Hess, S.T., Holowka, D.A., Baird, B.A., and Webb, W.W. (2007). Large-scale fluid/fluid phase separation of proteins and lipids in giant plasma membrane vesicles. PNAS *104*, 3165–3170.

Berndl, K., Käs, J., Lipowsky, R., Sackmann, E., and Seifert, U. (1990). Shape transformations of giant vesicles: extreme sensitivity to bilayer asymmetry. Europhys. Lett. *13*, 659–664.

Bo, L. and Waugh, R.E. (1989). Determination of bilayer membrane bending stiffness by tether formation from giant, thin-walled vesicles. Biophys. J. *55*, 509–517.

Breidenich, M., Netz, R., and Lipowsky, R. (2000). The shape of polymer-decorated membranes. Europhys. Lett. *49*, 431–437.

Choudhuri, K. and Dustin, M.L. (2010). Signaling microdomains in T cells. FEBS Lett. *584*, 4823–4831.

Collins, M.D. and Keller, S.L. (2008). Tuning lipid mixtures to induce or suppress domain formation across leaflets of unsupported asymmetric bilayers. PNAS *105*, 124–128.

Dalmédico, A. (1991). Sophie Germain. Sci. Am. *265*, 117–122.

David, J.H., Clair, J.J., and Juhasz, J. (2009). Phase equilibria in DOPC/DPPC-d62/cholesterol mixtures. Biophys. J. *96*, 521–539.

Dietrich, C., Bagatolli, L., Volovyk, Z., Thompson, N., Levi, M., Jacobson, K., and Gratton, E. (2001). Lipid rafts reconstituted in model membranes. Biophys. J. *80*, 1417–1428.

Dimova, R. and Lipowsky, R. (2012). Lipid membranes in contact with aqueous phases of polymer solutions. Soft Matter *8*, 6409–6415.

Dimova, R., Riske, K.A., Aranda, S., Bezlyepkina, N., Knorr, R.L., and Lipowsky, R. (2007). Giant vesicles in electric fields. Soft Matter *3*, 817–827.

Döbereiner, H.-G., Evans, E., Kraus, M., Seifert, U., and Wortis, M. (1997). Mapping vesicle shapes into the phase diagram: a comparison of experiment and theory. Phys. Rev. E *55*, 4458–4474.

Döbereiner, H.G., Selchow, O., and Lipowsky, R. (1999). Spontaneous curvature of asymmetric bilayer membranes. Eur. Biophys. J. *28*, 174–178.

Döbereiner, H.-G., Gompper, G., Haluska, C.K., Kroll, D.M., Petrov, P.G., and Riske, K.A. (2003). Advanced flicker spectroscopy of fluid membranes. Phys. Rev. Lett. *91*, 048301.

Domanov, Y.A. and Kinnunen, P.K.J. (2006). Antimicrobial peptides temporins B and L induce formation of tubular lipid protrusions from supported phospholipid bilayers. Biophys. J. *91*, 4427–4439.

Domingues, T.M., Riske, K.A., and Miranda, A. (2010). Revealing the lytic mechanism of the antimicrobial peptide gomesin by observing giant unilamellar vesicles. Langmuir *26*, 11077–11084.

Farsad, K., Ringstad, N., Takei, K., Floyd, S.R., Rose, K., and Camilli, P.D. (2001). Generation of high curvature membranes mediated by direct endophilin bilayer interactions. J. Cell Biol. *155*, 193–200.

Ford, M.G.J., Mills, I.G., Peter, B.J., Vallis, Y., Praefcke, G.J.K., Evans, P.R., and McMahon, H.T. (2002). Curvature of clathrin-coated pits driven by epsin. Nature *419*, 361–366.

Fourcade, B., Miao, L., Rao, M., Wortis, M., and Zia, R. (1994). Scaling analysis of narrow necks in curvature models of fluid lipid–bilayer vesicles. Phys. Rev. E *49*, 5276–5286.

Frank, F.C. (1958). Liquid crystals i: on the theory of liquid crystals. Discuss. Faraday Soc. *25*, 19–28.

Frost, A., Unger, V.M., and Camilli, P.D. (2009). The bar domain superfamily: Membrane-molding macromolecules. Cell *137*, 191–196.

Garg, S., Rühe, J., Lüdtke, K., Jordan, R., and Naumann, C.A. (2007). Domain registration in raft-mimicking lipid mixtures studied using polymer-rethered lipid bilayers. Biophys. J. *92*, 1263–1270.

Goetz, R., Gompper, G., and Lipowsky, R. (1999). Mobilitiy and elasticity of self-assembled membranes. Phys. Rev. Lett. *82*, 221–224.

Góźdź, W.T. and Gompper, G. (2001). Shape transformations of two-component membranes under weak tension. Europhys. Lett. *55*, 587–593.

Harden, J.L., MacKintosch, F.C., and Olmsted, P.D. (2005). Budding and domain shape transformations in mixed lipid films and bilayer membranes. Phys. Rev. *E 72*, 011903.

Helfrich, W. (1973). Elastic properties of lipid bilayers: theory and possible experiments. Z. Naturforsch. *28c*, 693–703.

Hochmuth, R.M., Shao, J.-Y., Dai, J., and Sheetz, M.P. (1996). Deformation and flow of membrane into tethers extracted from neuronal growth cones. Biophys. J. *70*, 358–369.

Ipsen, J.H., Karlström, G., Mouritsen, O.G., Wennerström, H., and Zuckermann, M.J. (1987). Phase equilibria in the phosphatidylcholine-cholesterol system. Biochim. Biophys. Acta *905*, 162–172.

Jensen, M.H., Morris, E.J., and Simonsen, A.C. (2007). Domain shapes, coarsening, and random patterns in ternary membranes. Langmuir *23*, 8135–8141.

Jülicher, F. and Lipowsky, R. (1993). Domain-induced budding of vesicles. Phys. Rev. Lett. *70*, 2964–2967.

Jülicher, F. and Lipowsky, R. (1996). Shape transformations of inhomogeneous vesicles with intramembrane domains. Phys. Rev. E *53*, 2670–2683.

Kiessling, V., Wan, C., and Tamm, L.K. (2009). Domain coupling in asymmetric lipid bilayers. Biochim. Biophys. Acta *1788*, 64–71.

Klasczyk, B., Knecht, V., Lipowsky, R., and Dimova, R. (2010). Interactions of alkali metal chlorides with phosphatidylcholine vesicles. Langmuir *26*, 18951–18958.

Knorr, R.L., Dimova, R., and Lipowsky, R. (2012). Curvature of double-membrane organelles generated by changes in membrane size and composition. PLoS One *7*, e32753.

Koster, G., Duijn, M.V., Hofs, B., and Dogterom, M. (2003). Membrane tube formation from giant vesicles by dynamic association of motor proteins. PNAS *100*, 15583–15588.

Kumar, S., Gompper, G., and Lipowsky, R. (2001). Budding dynamics of multicomponent membranes. Phys. Rev. Lett. *86*, 3911–3914.

Kusumaatmaja, H., Li, Y., Dimova, R., and Lipowsky, R. (2009). Intrinsic contact angle of aqueous phases at membranes and vesicles. Phys. Rev. Lett. *103*, 238103.

Leduc, C., Campas, O., Zeldovich, K., Roux, A., Jolimaitre, P., Bourel-Bonnet, L., Goud, B., Joanny, J.-F., Bassereau, P., and Prost, J. (2004). Cooperative extraction of membrane nanotubes by molecular motors. PNAS *101*, 17096–17101.

Li, Y., Lipowsky, R., and Dimova, R. (2011). Membrane nanotubes induced by aqueous phase separation and stabilized by spontaneous curvature. Proc. Natl. Acad, Sci. USA *108*, 4731–4736.

Lipowsky, R. (1991). The conformation of membranes. Nature *349*, 475–481.

Lipowsky, R. (1992). Budding of membranes induced by intramembrane domains. J. Phys. II France *2*, 1825–1840.

Lipowsky, R. (1995). Bending of membranes by anchored polymers. Europhys. Lett. *30*, 197–202.

Lipowsky, R. (2013). Spontaneous tubulation of membranes and vesicles reveals membrane tension generated by spontaneous curvature. Faraday Discuss. *161*, 305–331.

Lipowsky, R. and Dimova, R. (2003). Domains in membranes and vesicles. J. Phys. Cond. Mat. *15*, S31–S45.

Lipowsky, R. and Döbereiner, H.G. (1998). Vesicles in contact with nanoparticles and colloids. Europhys. Lett. *43*, 219–225.

Lipowsky, R., Rouhiparkouhi, T., Discher, D.E., and Weikl, T.R. (2013). Domain formation in cholesterol/phospholipid membranes exposed to adhesive surfaces or environments. Soft Matter *9*, 8438–3453.

Mally, M., Majhenc, J., Svetina, S., and Zeks, B. (2007). The response of giant phospholipid vesicles to pore-forming peptide melittin. Biochim. Biophys. Acta *1768*, 1179–1189.

Marsh, D. (2010). Liquid-ordered phases induced by cholesterol: a compendium of binary phase diagrams. Biochim. Biophys. Acta *1798*, 688–699.

McMahon, H.T. and Gallop, J.L. (2005). Membrane curvature and mechanisms of dynamic cell membrane remodelling. Nature *438*, 590–596.

Miao, L., Seifert, U., Wortis, M., and Döbereiner, H.-G. (1994). Budding transitions of fluid–bilayer vesicles: the effect of area–difference elasticity. Phys. Rev. E *49*, 5389–5407.

Nikolov, V., Lipowsky, R., and Dimova, R. (2007). Behavior of giant vesicles with anchored DNA molecules. Biophys. J. *92*, 4356–4368.

Orth, A., Johannes, L., Römer, W., and Steinem, C. (2012). Creating and modulating microdomains in pore-spanning membranes. Chem.Phys.Chem. *13*, 108–114.

Peter, B.J., Kent, H.M., Mills, I.G., Vallis, Y., Butler, P.J.G., Evans, P.R., and McMahon, H.T. (2004). BAR domains as sensors of membrane curvature: the amphiphysin BAR structure. Science *303*, 495–499.

Recktenwald, D.J. and McConnell, H.M. (1981). Biochemistry *20*, 4505–4510.

Reynwar, B.J., Illya, G., Harmandaris, V.A., Müller, M.M., Kremer, K., and Deserno, M. (2007). Aggregation and vesiculation of membrane proteins by curvature-mediated interactions. Nature *447*, 461–464.

Rouhiparkouhi, T., Weikl, T.R., Discher, D.E., and Lipowsky, R. (2013). Adhesion-induced phase behavior of two-component membranes and vesicles. Int. J. Mol. Sci. *14*, 2203–2229.

Sankaram, M.B. and Thompson, T.E. (1990). Interaction of cholesterol with various glycerophospholipids and sphingomyelin. Biochemistry *29*, 10670–10675.

Seifert, U. and Lipowsky, R. (1990). Adhesion of vesicles. Phys. Rev. A *42*, 4768–4771.

Seifert, U., Berndl, K., and Lipowsky, R. (1991). Shape transformations of vesicles: phase diagram for spontaneous curvature and bilayer coupling model. Phys. Rev. A *44*, 1182–1202.

Semrau, S., Idema, T., Holtzer, L., Schmidt, T., and Storm, C. (2008). Accurate determination of elastic parameters for multi-component membranes. Phys. Rev. Lett. *100*, 088101.

Simons, K. and Ikonen, E. (1997). Functional rafts in cell membranes. Nature *387*, 569–572.

Sorre, B., Callan-Jones, A., Manzi, J., Goud, B., Prost, J., Bassereau, P., and Roux, A. (2012). Nature of curvature coupling of amphiphysin with membranes depends on its bound density. PNAS *109*, 173–178.

Takei, K., Slepnev, V.I., Haucke, V., and Camilli, P.D. (1999). Functional partnership between amphiphysin and dynamin in clathrin-mediated endocytosis. Nat. Cell Biol. *1*, 33–39.

Veatch, S. and Keller, S. (2003). Separation of liquid phases in giant vesicles of ternary mixtures of phospholipids and cholesterol. Biophys. J. *85*, 3074–3083.

Veatch, S.L., Cicuta, P., Sengupta, P., Honerkamp-Smith, A., Holowka, D., and Baird, B. (2008). Critical fluctuations in plasma membrane vesicles. ACS Chem. Biol. *3*, 287–293.

Vist, M.R. (1984). Master's thesis (University of Guelph, Guelph, Ontario, Canada).

Vist, M.R. and David, J.H. (1990). Phase equilibria of cholesterol/dipalmitoylphosphatidylcholine mixtures: 2H nuclear magnetic resonance and differential scanning calorimetry. Biochemistry *29*, 451–464.

Wang, Q., Navarro, V.A.S., Peng, G., Molinelli, E., Goh, S.L., Judson, B.L., Rajashankar, K.R., and Sondermann, H. (2009). Molecular mechnism of membrane constriction and tubulation mediated by the F-BAR protein Pacsin/Syndapin. PNAS *106*, 1270s0–12705.

Weikl, T. and Lipowsky, R. (2004). Pattern formation during T cell adhesion. Biophys. J. *87*, 3665–3678.

Willmore, T. (1982). Total Curvature in Riemannian Geometry (Chicester: Ellis Horwood).

Zhu, C., Das, S.L., and Baumgart, T. (2012). Nonlinear sorting, curvature generation, and crowding of endophilin N-bar on tubular membranes. Biophys. J. *102*, 1837–1845.